Joint Rigid Registration of Multiple Generalized Point Sets With Anisotropic Positional Uncertainties in Image-Guided Surgery

Zhe Min, *Member, IEEE*, Jiaole Wang, *Member, IEEE*, and Max Q.-H. Meng, *Fellow, IEEE*

***Abstract*— In medical image analysis (MIA) and computer-assisted surgery (CAS), aligning two multiple point sets (PSs) together is an essential but also a challenging problem. For example, rigidly aligning multiple point sets into one common coordinate frame is a prerequisite for statistical shape modelling (SSM). Accurately aligning the pre-operative space with the intra-operative space in CAS is very crucial to successful interventions. In this article, we formally formulate the multiple generalized point set registration problem (MGPSR) in a probabilistic manner, where both the positional and the normal vectors are used. The six-dimensional vectors consisting of both positional and normal vectors are called as generalized points. In the formulated model, all the generalized PSs to be registered are considered to be the realizations of underlying unknown hybrid mixture models (HMMs). By assuming the independence of the positional and orientational vectors (i.e., the normal vectors), the probability density function (PDF) of an observed generalized point is computed as the product of Gaussian and Fisher distributions. Furthermore, to consider the anisotropic noise in surgical navigation, the positional error is assumed to obey a multi-variate Gaussian distribution. Finally, registering PSs is formulated as a maximum likelihood (ML) problem, and solved under the expectation maximization (EM) technique. By using more enriched information (i.e., the normal vectors), our algorithm is more robust to outliers. By treating all PSs equally, our algorithm does not bias towards any PS. To validate the proposed approach, extensive experiments have been conducted on surface points extracted from CT images of (i) a human femur bone model; (ii) a human pelvis bone model. Results demonstrate our algorithm's high accuracy, robustness to noise and outliers.**

***Note to Practitioners*—This paper was motivated by solving the problem of registering two or more PSs. Most existing registration approaches use only the positional information associated with each point, and thus lacks robustness to noise and outliers. Three significant improvements are brought by our proposed approach. First, the normal vectors that can be extracted from the point sets are utilized in the registration. Second, the positional error distribution is assumed to be anisotropic *and* inhomogeneous. Third, all the PSs to be registered are treated equally that means no PS is considered as the model one. The registration problem is cast into a maximum likelihood (ML) problem and solved under the expectation maximization (EM) framework. We have demonstrated through extensive experiments that the proposed registration approach achieves significantly improved accuracy, robustness to noise and outliers. The algorithm is particularly suitable for biomedical applications involving the registration procedures, such as image-guided surgery.**

***Index Terms*— Healthcare and life sciences, image-guided surgery, surgical navigation, biomedical engineering.**

I. Introduction

POINT set registration (PSR) is a fundamental and challenging problem in the fields of medical robotics, medical image analysis (MIA) and computer-assisted surgery (CAS) [1]–[15]. The aim of the rigid PSR problem is to accurately compute the rigid transformation matrix between point sets (PSs) [2]. In CAS, both *fiducial-based registration* and *surface registration* (or generally speaking PSR) can be used to align the pre-operative volumetric image space to the intra-operative patient space [16]–[18]. In *fiducial-based registration*, a few fiducials (anatomical landmarks or artificial markers) with known correspondences in two spaces are used [19], [20]. In *surface registration*, surface points without correspondences in two spaces are used. For example, in computer-assisted total hip replacement (THR) surgery, the intra-operative points acquired with a tracked pointer are registered to the surface points extracted from the CT model of the patient's bone, where a surface can be represented by either a PS or a mesh [21], [22].

The possible clinical applications of the registration problem to be dealt with in this article are summarized as follows. (1) Pre-operative to intra-operative space alignment in

Manuscript received October 19, 2020; revised March 13, 2021, July 28, 2021, and October 8, 2021; accepted November 5, 2021. This article was recommended for publication by Associate Editor K. Paynabar upon evaluation of the reviewers' comments. This work was supported in part by the Hong Kong Research Grants Council (RGC) General Research Fund (GRF) under Grant 14210117 and Grant 14211420, in part by the RGC NSFC/RGC Joint Research Scheme under Grant N_CUHK448/17, in part by the National Key Research and Development Program of China under Grant 2019YFB1312400, and in part by the Shenzhen Science and Technology Innovation Projects under Grant JCYJ20170413161503220. The work of Max Q.-H. Meng was supported in part by the Hong Kong RGC Theme-Based Research Scheme (TRS) under Grant T42-409/18-R. *(Corresponding author: Max Q.-H. Meng.)*

Zhe Min is with the Department of Medical Physics and Biomedical Engineering, University College London, London WC1E 6BT, U.K. (e-mail: zhemincuhk@gmail.com).

Jiaole Wang is with the School of Mechanical Engineering and Automation, Harbin Institute of Technology, Shenzhen 518052, China (e-mail: wangjiaole@hit.edu.cn).

Max Q.-H. Meng is with the Department of Electronic and Electrical Engineering, Southern University of Science and Technology, Shenzhen 518055, China, on leave from the Department of Electronic Engineering, The Chinese University of Hong Kong, Hong Kong, and also with the Shenzhen Research Institute, The Chinese University of Hong Kong, Shenzhen 518057, China (e-mail: max.meng@ieee.org).

Color versions of one or more figures in this article are available at https://doi.org/10.1109/TASE.2021.3127172.

Digital Object Identifier 10.1109/TASE.2021.3127172

CAS [2], [17], [23], [24]. (2) Statistical shape modelling (SSM). Statistical shape models (SSMs) are important and powerful tools for various medical image analysis applications such as automatic segmentation of important organs [25]. Generally speaking, SSMs describe the variation in the shape of an object about a mean shape representation of the population. As summarized in [26], shapes can be represented by *point set*, *mesh*, implicit functions (*signed distance maps*), *spherical harmonics (SPHARM) based parametrization and medial shape representation*. Rigidly aligning PSs into one common coordinate frame is the first and a very important step of accurately constructing the SSM [27]. The first important step in constructing the SSMs from population data is to exclude the global pose differences of the training samples, which include the rotation matrix, translation vector and scaling factor [26]. Basically speaking, two general frameworks are utilized in building SSMs. (i) The *pair-wise registration strategy* where a reference is non-rigidly registered to each training sample; (ii) the *group-wise registration strategy* where multiple point sets are *jointly* registered and point correspondences are also estimated. The registration biased towards the reference point set when the first strategy is used.

This article is motivated by the following three aspects. (1) In order to significantly improve the registration accuracy and robustness, we utilize the orientation-al information (i.e., the normal vectors) that can be extracted from the raw PS with various methods [2], [28], [29]. (2) The second motivation is to consider the anisotropic characteristic in the position localization error, which is common in many CAS applications [29]–[32]. (3) The third motivation is to remove the bias towards one specific PS in the PSR algorithm. In both Iterative Closest Point (ICP)-based and Gaussian Mixture Model (GMM)-based registration methods, there is a bias towards one PS [33], [34].

Our contributions of this article are summarized as follows.

1) The *anisotropic* position localization error (PLE) is considered in the joint rigid registration of multiple generalized point sets. Thus, the JRMPC framework is generalized to the six-dimensional case where anisotropic PLE is considered.
2) In the case of registering multiple point sets, we reformulate the constrained optimization problem of updating the rotation matrix, in the maximization step, to an unconstrained one by using the Rodrigues Formula to represent the rotation. The gradients of the objective function with respect to the desired parameters are computed and provided, in order to speed up the computational process.

The remainder of this article is organized as follows. Section. II reviews the related registration methods. Section. III formally formulates the multiple generalized point set registration (MGPSR) problem. Section. IV describes our algorithm in details. Section. V gives a summary of the two expriments. Section. VI presents the first experiment and its results. Section. VII presents the second experiment and its results. Section. VIII presents the discussion of this paper. Finally, Section IX concludes the article.

II. Related Work

We review the probabilistic registration methods in the following. Some recent deep learning based methods are also briefly covered.

A. Probabilistic Registration Methods

There exists a large amount of work that tries to solve the PSR problem [3]. Many probabilistic methods have been proposed to overcome the drawbacks of the ICP-like method [3]. The strategy of assigning soft-correspondence between one point in one PS to several points in the other PS is often used in this category. Registration is formulated as a Maximum Likelihood Estimation (MLE) problem and solved using the Expectation Maximization (EM) technique [3]. In an EM-based registration algorithm, each iteration consists of two steps [33]. That is (i) E-step, the posteriors indicating the correspondence confidence between points in two PSs are computed; (ii) M-step, the best rigid transformation matrix is estimated given the current posteriors. The above two steps will iterate until some termination conditions are satisfied. Finally, the 'best' rigid transformation matrix relating two PSs is calculated after conducting the above two steps for a while.

As a typical representation of the probabilistic methods, in the coherent point drift (CPD) method [33], one PS (representing the data shape) is considered to be the sampled transformed/misaligned GMMs whose means are the points in the other PS (representing the model shape). The readers should note that there is a bias assuming that one PS(i.e., the model PS) is perfect without error. In the GMMReg method [35], both PSs to be registered are represented as GMMs and the *L2* distance between the two mixtures is minimized in order to compute the rigid transformation matrix. Expectation conditional maximization point registration (ECMPR) method utilizes a general covariance matrix for the mixture model under a similar statistical framework as that is used in CPD [36]. They re-formulate the nonlinear problem of computing the rotation matrix into a constrained quadratic optimization problem and used the semidefinite positive relaxation (SEM) technique to solve it [36]. In all the above three methods [33], [35], [36], the bias towards one PS in the registration process exists [34].

We now review the methods for multi-view or multiple PSR problem. Three categories of registration methods are presented as follows. (i) With the strategy of sequential pairwise registration, register-then-integrate processes are repeated until all the PSs are utilized [37]–[39]. In other words, whenever an additional PS is available, the model PS is updated repeatedly. The main drawback of methods in this category is that the registration error will accumulate [34]. (ii) Motion averaging technique [40] and the rotation averaging method [41] have also been used to register multiple PSs. In the Motion Averaging Iterative Closest Point (MA-ICP) algorithm, the Lie-algebraic averaging of relative motions is used to compute the global motions for each view [40]. Two drawbacks exist in the MA-ICP algorithm [34]: a) The topology needs to be known or estimated; b) The closed-loop constraint is required. (iii) Similar to [35], in [42] each PS is represented

as a respective GMM and the non-rigid transformation is applied to the multiple mixture centers rather than the points directly. The mixture model's parameters are estimated by minimizing the Jensen-Shannon divergence. A probabilistic mean shape is computed as the convex combination of the already aligned PSs. The main disadvantage of this method is that it requires the PSs to be well structured [42]. Recently, to tackle the shortcomings of the GMM-based statistical registration algorithm including slow speed and lack of generality, Eckart *et al.* constructs a top-down multi-scale representation of PS data by recursively running many small-scale data likelihood segmentations in parallel on a GPU [43]. To enhance the registration performance particularly in cases of large-pose displacements and non-overlapping geometry, the overlapping regions are estimated through a expectation maximization procedure [44]. The estimated non-overlapping regions can be further down-weighted or ignored in the data association process [44]. Gao *et al.* formulates the E step as a filtering problem and solve it using advances in efficient Gaussian filters, which can help the registration achieve good robustness and efficiency [45].

More recently, the joint registration of multiple point clouds (JRMPC) method is proposed to remove the bias towards one specific PS in the registration process [34]. In the JRMPC method [34], all PSs to be registered are regarded as the transformed realizations of underlying unknown GMMs. In this way, there is no bias towards any specific PS in JRMPC. JRMPC outperforms or is comparable to the state-of-the-art algorithms such as CPD [33], GMMReg [35], ECMPR [36] and SimReg [46] under various levels of isotropic noise and different outliers conditions. We should note that one main drawback of the JRMPC method is that the positional error obeys the isotropic Gaussian distribution.

The non-rigid registration with the hybrid mixture models (HMMs) have been proposed by researchers [47]–[49]. The Student t distribution models are used to model the positional error while the uncertainties with the normal vectors are modelled with Fisher mixture models (FMMs) [47], [48]. In [47], Ravikumar *et al.* have formulated and solved the group-wise registration problem with normal vectors for both rigid and non-rigid registration problems. The pair-wise registration method similar to [47] was used in the vascular-based registration framework, where the normal vectors' uncertainties are modelled with the Watson distributions. In [49], the deformable registration problem is formulated and used for the endoscopic navigation. More specifically, the patient to be treated does not need to undergo the CT scanning and thus lacks the pre-operative CT data. Statistical shape models (SSMs) are first constructed from other patients' CT scan data. The intra-operative 3D surface data is non-rigidly registered with the SSMs. Basically speaking, the registration method in [49] is a pair-wise one where the bias towards one specific PS exists. Additionally, the ICP framework is used in [49] and thus the robustness to outliers can be further improved. One potential limitation of the method in [47] is that the positional uncertainty is assumed to be isotropic.

B. Deep Learning-Based Registration Methods

There are some deep learning-based registration methods developed for PSR. Most of those work focuses on developing novel methods to first learn compact local descriptors of the PSs [50]–[53]. Deng *et al.* present the PPFNet framework that can fast learns the local patch descriptor, which is highly aware of the global context and has increased tolerance to rotations [54]. Zan *et al.* use a smoothed density value (SDV) voxelization as the input data representation to the standard deep-learning libraries [55]. They also present a novel network architecture that learns a very compact, rotation invariant 3D local feature descriptor, which is low dimensional and has been demonstrated to speed up the correspondence search and thus allows real-time applications.

Current deep-learning based registration methods are not robust to outliers, which usually exist in the applications of image-guided surgery (IGS) [56]. Deep-learning methods neither guarantee the registration accuracy nor provide the threshold of the registration error. In contrast, the target registration error (TRE) model can estimate the registration error's magnitudes and covariance matrix given the fiducial localization error (FLE) [16], [31]. In addition, there are also models that estimate the upper bounds of the registration error. The above-mentioned error estimation/prediction models are only valid for methods such as ICP or the probabilistic methods(i.e., ECMPR and JRMPC methods).

C. Differences/Improvements Compared With Our Previous Work

The main/significant differences or improvements of our presented work with our previous work [57] include the follows. Scientifically (i) The positional error distribution is assumed to be anisotropic while the normal vectors extracted from the raw point sets are utilized in the simultaneous registration of multiple point sets, whereas the isotropic positional error is assumed in our previous work; Technically (ii) Both cases where the isotropic and anisotropic positional error vectors are injected into the point sets have been tested, whereas only the case of isotropic positional error is considered in our previous work; (iii) We have explored the influences of the hyperparameters including the weight of the outlier distribution in the hybrid mixture models(HMMs) and the number of central models' components on the registration performance; (iv) We have evaluated the registration performances under different magnitudes of noise injected into normal vectors(i.e., different values of the concentration parameter κ).

III. Problem Formulation

Let $\mathbf{D}_j = [\mathbf{d}_{j1} \dots \mathbf{d}_{ji} \dots \mathbf{d}_{jN_j}] \in \mathbb{R}^{6\times N_j}$ be the set containing N_j observed generalized points in the j-th PS, and N be the number of all PSs (or views) to be registered. More specifically, we denote the generalized point $\mathbf{d}_{ji} = (\mathbf{x}_{ji}; \widehat{\mathbf{x}}_{ji})$, where $\mathbf{x}_{ji} \in \mathbb{R}^{3\times 1}$ and $\widehat{\mathbf{x}}_{ji} \in \mathbb{R}^{3\times 1}$(is a unit vector) respectively represent the positional and normal vectors of the i-th generalized point in the j-th PS $\mathbf{D}_j$. For clarity, we denote

$\mathbf{D} = \{\mathbf{D}_j\}_{j=1}^{N}$ as the union of all PSs to be registered. In our method, all the observed PSs $\mathbf{D}$ are considered to be the transformed realizations (samples) from the underlying hybrid mixture models (HMMs), whose centroids are actually the underlying central generalized PS. The aim of the multiple generalized point set registration (MGPSR) problem is to find the 'best' rotation matrix set $\{\mathbf{R}_j\}_{j=1}^{N}$ and translation vector set $\{\mathbf{t}_j\}_{j=1}^{N}$ that align the unknown central model PS $\{\mathbf{d}_m \in \mathbb{R}^{6\times 1}\}_{m=1}^{M}$ ($\mathbf{d}_m = (\mathbf{y}_m; \widehat{\mathbf{y}}_m)$) with $\{\mathbf{D}_j\}_{j=1}^{N}$, where M is the number of points in the underlying model PS.

Two assumptions are adopted in this work: (i) the positional and normal vectors are independent; (ii) the localization error of the positional and the normal vectors respectively obey the multi-variate Gaussian distribution and the von-Mises-Fisher [58] distribution respectively. A brief introduction of von-Mises Fisher distribution is provided in Appendix. B. The adopted multi-variate Gaussian distribution generalizes the isotropic positional error distribution in our previous work [57]. The model parameters Θ in our algorithm are summarized as

$$\Theta = (\{\mathbf{R}_j, \mathbf{t}_j, \kappa_j, \Sigma_j\}_{j=1}^{N}, \{\mathbf{d}_m\}_{m=1}^{M}) \tag{1}$$

where we note that every $\mathbf{D}_j (j = 1, \ldots, N)$ owns its specific positional covariance matrix $\Sigma_j \in \mathbb{S}^{3\times 3}$ and concentration parameter $\kappa_j \in \mathbb{R}^3$. We provide a brief introduction of JRMPC method in Appendix. C.

Let $\mathcal{Z} = \{z_{ji} | j \in [1 \ldots N], i \in [1 \ldots N_j]\}$ denote the hidden/latent variables set, where $z_{ji} = m$ indicates that the m-th component of HMMs generates the point $\mathbf{d}_{ji}$. The marginal distribution $p(\mathbf{d}_{ji}|\Theta)$ of an observed generalized point $\mathbf{d}_{ji}$ under Θ is

$$p(\mathbf{d}_{ji}|\Theta) = \sum_{m=1}^{M+1} P(m)\, p(\mathbf{d}_{ji}|z_{ji} = m, \Theta_{jm}) \tag{2}$$

where $\Theta_{jm} = \{\mathbf{R}_j, \mathbf{t}_j, \kappa_j, \Sigma_j, \mathbf{d}_m\}$, and the probability density function (PDF) describing the probability that $\mathbf{d}_{ji}$ corresponds to the m-th HMMs component ($m = 1, \ldots, M$) is

$$\begin{aligned} &p(\mathbf{d}_{ji}|z_{ji} = m, \Theta_{jm}) \\ &= \underbrace{\frac{1}{(2\pi)^{\frac{3}{2}}|\Sigma_j|^{\frac{1}{2}}} e^{\frac{-1}{2}\mathbf{z}_{jim}^{\mathsf{T}}\Sigma_j^{-1}\mathbf{z}_{jim}}}_{Gaussian} \underbrace{\frac{\kappa_j}{2\pi(e^{\kappa_j} - e^{-\kappa_j})} e^{\kappa_j(\mathbf{R}_j\widehat{\mathbf{y}}_m)^{\mathsf{T}}\widehat{\mathbf{x}}_{ji}}}_{Fisher} \\ &= \frac{\kappa_j}{(2\pi)^{\frac{5}{2}}|\Sigma_j|^{\frac{1}{2}}(e^{\kappa_j} - e^{-\kappa_j})} e^{\kappa_j(\mathbf{R}\widehat{\mathbf{y}}_m)^{\mathsf{T}}\widehat{\mathbf{x}}_{ji} - \frac{1}{2}(\mathbf{z}_{jim})^{\mathsf{T}}\Sigma_j^{-1}(\mathbf{z}_{jim})} \end{aligned} \tag{3}$$

where $\mathbf{z}_{jim} = \mathbf{x}_{ji} - \mathbf{R}_j\mathbf{y}_m - \mathbf{t}_j$ denotes the distance vector between $\mathbf{x}_{ji}$ and transformed model point $\mathbf{y}_m$, and $|\bullet| = \det(\bullet)$ is the determinant of a square matrix. The readers should note that the term $\frac{1}{(2\pi\sigma_m^2)^{\frac{3}{2}}} e^{-\frac{1}{2\sigma_m^2}||\mathbf{x}_{ji} - \mathbf{R}\mathbf{y}_m - \mathbf{t}||^2}$ in (14) or (3) in [57] is replaced with $\frac{1}{(2\pi)^{\frac{3}{2}}|\Sigma_j|^{\frac{1}{2}}} e^{\frac{-1}{2}\mathbf{z}_{jim}^{\mathsf{T}}\Sigma_j^{-1}\mathbf{z}_{jim}}$. The rationale of (3) is summarized as follows. The transformed m-th position vector in the central PS into the coordinate frame associated with $\mathbf{D}_j$, $\mathbf{R}_j\mathbf{y}_m + \mathbf{t}_j$, is assumed to be the Gaussian Mixture Models's one centroid. More specifically, given $z_{ji} = m$, the data point $\mathbf{x}_{ji}$ is assumed to be one random sample from the Gaussian distribution centred at $\mathbf{R}_j\mathbf{y}_m + \mathbf{t}_j$, i.e., $\mathcal{N}(\mathbf{R}_j\mathbf{y}_m + \mathbf{t}_j, \Sigma_j)$. At the same time, the transformed m-th normal vector in the central PS into the coordinate frame associated with $\mathbf{D}_j$, $\mathbf{R}_j\widehat{\mathbf{y}}_m$, is assumed to be the Fisher Mixture Model's one central direction. More specifically, given $z_{ji} = m$, the data normal vector $\widehat{\mathbf{y}}_{ji}$ is assumed to be one random sample from the Fisher distribution centred at $\mathbf{R}_j\widehat{\mathbf{y}}_m$, i.e. $\mathcal{F}(\mathbf{R}_j\widehat{\mathbf{y}}_m, \kappa)$. With the independence between the positional vectors and normal vectors, the probability of a data point $\mathbf{d}_{ji}$ being generated by the m-th central point $\mathbf{d}_m$ is the product of the Gaussian and Fisher probability densities. To account for noise and outliers, one uniform distribution $p(\mathbf{d}_{ji}|z_{ji} = M + 1) = \frac{1}{N_j}$ is included in the model in (2). Equal (symmetrical) membership probabilities $P(m) = \frac{1}{M}$ are assumed for all the remaining HMMs' components (i.e. $m = 1, \cdots, M$). Then we can expand $p(\mathbf{d}_{ji}|\Theta_{jm})$ in (2) as

$$p(\mathbf{d}_{ji}|\Theta_{jm}) = w\frac{1}{N_j} + (1 - w)\sum_{m=1}^{M}\frac{1}{M}p(\mathbf{d}_{ji}|z_{ji} = m, \Theta_{jm}), \tag{4}$$

where $0 \leq w \leq 1$ is the weight of the additional uniform distribution. With the assumption that each $\mathbf{d}_{ji}$ are independent with each other, the PDF of the $\mathbf{D}$ given the model parameters Θ is in fact the product of individual probabilities $p(\mathbf{D}, \mathcal{Z}|\Theta) = \prod_{ji} p(\mathbf{d}_{ji}|z_{ji}, \Theta_{jm})$, where $p(\mathbf{d}_{ji}|z_{ji}, \Theta_{jm})$ is presented in (4).

A. Derivation of the Objective Function

The multiple generalized point set registration task is now performed by estimating the parameters Θ from the data PS $\mathbf{D}$. To find the optimal estimation of Θ is to minimize the expected negative log-likelihood term with respect to the latent variables $\mathcal{Z}$,

$$\begin{aligned} Q(\Theta|\mathbf{D}, \mathcal{Z}) &= \mathbb{E}_{\mathcal{Z}}[\log p(\mathbf{D}, \mathcal{Z}|\Theta] \\ &= \sum_{\mathcal{Z}} P(\mathcal{Z}|\mathbf{D}, \Theta)\log(p(\mathbf{D}, \mathcal{Z}; \Theta)), \end{aligned} \tag{5}$$

Expectation Maximization (EM) technique is used to estimate the parameters Θ in (1) in the case of hidden parameters. As indicated in [33], the idea of the EM technique is to guess the parameters' values and use the Bayes' theorem to compute the posteriors $\alpha_{jim} = P(z_{ji} = m|\mathbf{d}_{ji}, \Theta)$ of HMMs components, which is the expectation or E-step. The model parameters Θ values are then updated through minimizing the conditional expectation of the complete-data negative log-likelihood function [59]:

$$Q(\Theta|\mathbf{D}, \mathcal{Z}) = -\sum_{j=1}^{N}\sum_{i=1}^{N_j}\sum_{m=1}^{M+1}\alpha_{jim}\log p(\mathbf{d}_{ji}|z_{ji} = m; \Theta_{jm}), \tag{6}$$

with respect to the "new" parameters, which is the maximization or M-step of our algorithm. The objective function $Q(\Theta|\mathbf{D}, \mathcal{Z})$ in (6) is the upper bound of the negative log-likelihood function in (5) [59].

Ignoring the constants with respect to Θ, $Q(\Theta|\mathbf{D},\mathcal{Z})$ in (6) is expanded as follows,

$$\begin{aligned} f(\Theta) = &\sum_{jim}\alpha_{jim}\Big(\frac{1}{2}(\mathbf{z}_{jim})^{\mathsf{T}}\Sigma_j^{-1}(\mathbf{z}_{jim}) - \kappa_j\big((\mathbf{R}_j\widehat{\mathbf{y}}_m)^{\mathsf{T}}\widehat{\mathbf{x}}_{ji}\big)\Big) \\ &+\frac{1}{2}\sum_{j=1}^{N}N_{\mathbf{P}j}\log|\Sigma_j| + \sum_{j=1}^{N}N_{\mathbf{P}j}\log\left(e^{\kappa_j}-e^{-\kappa_j}\right) \\ &-\sum_{j=1}^{N}N_{\mathbf{P}j}\log\kappa_j, \end{aligned} \tag{7}$$

where $\alpha_{jim} = P(z_{ji}=m|\mathbf{d}_{ji},,\Theta)$, $N_{\mathbf{P}j} = \sum_{i=1}^{N_j}\sum_{m=1}^{M}\alpha_{jim}$. The objective function $f(\Theta)$ in (7) has to be minimized to find the model parameters Θ. We notice that the sum of the 'weighted distance' between positional vectors $\alpha_{jim}\frac{1}{2}(\mathbf{z}_{jim})^{\mathsf{T}}\Sigma_j^{-1}(\mathbf{z}_{jim})$ and 'weighted distance' between orientation-al vectors $-\alpha_{jim}\kappa_j\big((\mathbf{R}_j\widehat{\mathbf{y}}_m)^{\mathsf{T}}\widehat{\mathbf{x}}_{ji}\big)$ has to be minimized when we update the rigid transformation parameters $\{\mathbf{R}_j,\mathbf{t}_j\}_{j=1}^N$. The registration accuracy can thus be further improved since we utilize both positional and orientation-al information. Our algorithm's great robustness to outliers benefits from the following two aspects. (i) If α_{jim} will be computed to be small for $m=1,\ldots,M$, then one observed point $\mathbf{d}_{ji}$ is considered more likely to be an outlier. Thus, the contribution of one probable outlier will be smaller than probable inliers when we minimize $f(\Theta)$ in (7). (ii) The updated α_{jim} is subject to both positional and orientation-al information.

IV. Expectation Maximization for Multiple Generalized Point Set Registration

The posteriors are first found in the E-step in our algorithm. The model parameters Θ are updated in the three M-steps given the current posteriors $\{\alpha_{jim}^q\}$. (i) The M-rigid step minimizes $f(\Theta)$ in (7) with respect to the rigid transformation parameters $\{\mathbf{R}_j,\mathbf{t}_j\}_{j=1}^N$, given the current HMM parameters $\{\kappa_j^{q-1},\Sigma_j^{q-1}\}_{j=1}^N$. (ii) The M-cov step minimizes $f(\Theta)$ in (7) with respect to the HMM parameters $\{\kappa_j,\Sigma_j\}_{j=1}^N$, given the new values of the rigid transformation matrix $\{\mathbf{R}_j^q,\mathbf{t}_j^q\}_{j=1}^N$. (iii) The M-model step minimizes $f(\Theta)$ in (7) with respect to $\{\mathbf{d}_m\}_{m=1}^M$, given the current parameters $\{\mathbf{R}_j^q,\mathbf{t}_j^q,\kappa_j^q,\Sigma_j^q\}_{j=1}^N$.

A. E-Step

In this step, the posteriors that associate one observed generalized point $\mathbf{d}_{ji}$ with an underlying HMMs' component centroid $\mathbf{d}_m$, α_{jim}^q, are updated by using the Bayes' theorem: $\alpha_{jim}^q = P(\mathbf{z}_{ji}=m|\mathbf{d}_{ji},\Theta^{q-1}) = \frac{P(\mathbf{z}_{ji}=m)p(\mathbf{d}_{ji}|\mathbf{z}_{ji}=m,\Theta_{jm}^{q-1})}{p(\mathbf{d}_{ji}|\Theta^{q-1})}$, where $p(\mathbf{d}_{ji}|\mathbf{z}_{ji}=m,\Theta_{jm}^{q-1})$ and $p(\mathbf{d}_{ji}|\Theta^{q-1})$ are defined in (3) and (4), respectively.

B. M-Rigid Step

In this step, the rigid transformation matrix set $\{\mathbf{R}_j^q,\mathbf{t}_j^q\}_{j=1}^N$ is updated. In our previous work in [57] where the positional error is isotropic, $\mathbf{R}_j^q,\mathbf{t}_j^q$ have closed-form solutions. In contrast, there is no closed-form solution of the rigid transformation matrix when the positional error is generalized to the anisotropic case. This is because that two hard non-linear constraints of the rotation matrices to be satisfied in solving the optimization problem. Two proposed steps are involved to solve this problem: (1) formulate the optimization problem with respect to $[\mathbf{R}_j,\mathbf{t}_j]$ into another problem with respect to $[d\mathbf{R}_j,d\mathbf{t}_j]$; (2) based on the Rodrigues formula, the optimization problem with respect to $[d\mathbf{R}_j,d\mathbf{t}_j]$ reduces to another optimization problem with respect to a six-dimensional vector. The details are introduced as follows.

The rigid transformation matrix set $\{\mathbf{R}_j^q,\mathbf{t}_j^q\}_{j=1}^N$ is updated by minimizing $f(\Theta)$ in (7), given the current values for α_{jim}^q, κ_j^{q-1} and Σ_j^{q-1}. $f(\Theta)$ in (7) is minimized with respect to $\{\mathbf{R}_j,\mathbf{t}_j\}_{j=1}^N$ while considering two sets of non-linear constraints, namely (i) $\mathbf{R}_j^{\mathsf{T}}\mathbf{R}_j = \mathbf{I}_{3\times3}$ and (ii) $\det(\mathbf{R}_j)=1$. Let $[d\mathbf{R}_j^q,d\mathbf{t}_j^q]$ denote the incremental transformation matrix between two successive M-rigid steps (i.e. q and $q-1$ steps) associated with $\mathbf{D}_j$ in the q-th step. The optimization problem with respect to $[\mathbf{R}_j,\mathbf{t}_j]$ is reformulated to one optimization problem with respect to $[d\mathbf{R}_j,d\mathbf{t}_j]$ for $\mathbf{D}_j$ as the following

$$\begin{aligned}[d\mathbf{R}_j^q,d\mathbf{t}_j^q] = \arg\min_{d\mathbf{R}_j,d\mathbf{t}_j}\sum_{i,m=1}^{N_j,M}\Bigg(&\underbrace{\frac{1}{2}\alpha_{jim}^q(\mathbf{z}_{jim}^q)^{\mathsf{T}}\Sigma_j^{-1}(\mathbf{z}_{jim}^q)}_{\mathbf{C}_{P,jim}} \\ &\underbrace{-\alpha_{jim}^q\kappa_j^{q-1}(d\mathbf{R}_j\mathbf{R}_j^{q-1}\widehat{\mathbf{y}}_m)^{\mathsf{T}}\widehat{\mathbf{x}}_{ji}}_{\mathbf{C}_{N,jim}}\Bigg),\end{aligned} \tag{8}$$

where $\mathbf{z}_{jim}^q = \mathbf{x}_{ji} - d\mathbf{R}_j(\mathbf{R}_j^{q-1}\mathbf{y}_m^{q-1}+\mathbf{t}_j^{q-1}) - d\mathbf{t}_j$. We utilize the Rodrigues parametrization to represent the incremental rotation matrix $d\mathbf{R}_j$ associated with $\mathbf{D}_j$ between two adjacent steps. More specifically, the rotation matrix is represented as a three-element vector (i.e. $\boldsymbol{\theta} = [\theta_1,\theta_2,\theta_3]^{\mathsf{T}}$), whose direction and magnitude represent the axis and angular extent of rotation, respectively. The expression of the Rodrigues formula is presented in Appendix. E.

Let $\mathbf{b}_j \in \mathbb{R}^{6\times1}$ $(j=1,\ldots,N)$ be defined as $\mathbf{b}_j = [d\boldsymbol{\theta}_j^{\mathsf{T}},d\mathbf{t}_j^{\mathsf{T}}]^{\mathsf{T}}$, where $d\boldsymbol{\theta}_j \in \mathbb{R}^{3\times1}$ and $d\mathbf{t}_j \in \mathbb{R}^{3\times1}$. With the Rodrigues formula in (28), we can re-parametrize $[d\mathbf{R}_j,d\mathbf{t}_j]$ as a function of $\mathbf{b}_j$:

$$\begin{cases} d\mathbf{R}_j = \mathbf{R}(\mathbf{b}_j(1:3)), \\ d\mathbf{t}_j = \mathbf{b}_j(4:6), \end{cases} \tag{9}$$

where $\mathbf{b}_j(1:3) \in \mathbb{R}^{3\times1}$ and $\mathbf{b}_j(4:6) \in \mathbb{R}^{3\times1}$ represents the first three and last three elements of $\mathbf{b}_j$. After substituting the expression of $[d\mathbf{R}_j,d\mathbf{t}_j]$ in (9) into (8), computing the rigid transformation matrix $[\mathbf{R}_j^q,\mathbf{t}_j^q]$ in the q-th step turns to solving an unconstrained optimization problem with respect to the vector $\mathbf{b}_j$:

$$\mathbf{b}_j^q = \arg\min_{\mathbf{b}_j}\underbrace{\sum_{i=1}^{N_j}\sum_{m=1}^{M}\Big(\mathbf{C}_{P,jim}+\mathbf{C}_{N,jim}\Big)}_{\mathbf{C}_j}. \tag{10}$$

To solve the optimization problem in (10), the "fminunc" function in MATLAB with "trust-region" method is utilized. In order to speed up the computing process, we compute the

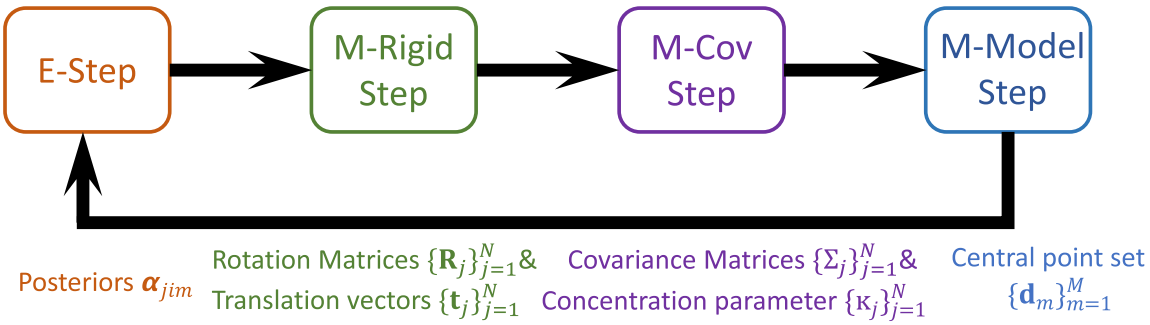

Fig. 1. The summarized procedure of our proposed point set registration algorithm. Each iteration in the proposed framework consists of four steps: (1) Expectation step (E-step) that the posterior correspondence probabilities are updated; (2) Maximization rigid (M-Rigid Step) that the rigid transformation matrix is updated; (3) Maximization covariance (M-Cov Step) that the positional covariance matrix is updated; (4) Maximization model (M-Model step) that the central unknown point set is updated.

gradients of $\mathbf{C}_j$ in (10) with respect to $\mathbf{b}_j$, $\nabla\mathbf{C}_j \in \mathbb{R}^{3\times 1}$: $\nabla\mathbf{C}_j = \sum_{i=1}^{N_j}\sum_{m=1}^{M}(\nabla\mathbf{C}_{P,jim} + \nabla\mathbf{C}_{N,jim})$, where

$$\begin{cases} \nabla\mathbf{C}_{P,jim} = [\mathbf{J}_{\mathbf{C}_{P,jim},d\boldsymbol{\theta}_j}, \mathbf{J}_{\mathbf{C}_{P,jim},d\boldsymbol{t}_j}]^{\mathsf{T}}, \\ \nabla\mathbf{C}_{N,jim} = [\mathbf{J}_{\mathbf{C}_{N,jim},d\boldsymbol{\theta}_j}, \mathbf{0}_{1\times 3}]^{\mathsf{T}}, \end{cases} \tag{11}$$

where $\mathbf{J}_{a,b}$ denotes the Jacobian of an expression a with respect to some variable b, and the three Jacobians in (11) are $\mathbb{R}^{1\times 3}$. After that $\boldsymbol{b}_j^q$ has been calculated, then $[d\mathbf{R}_j^q, d\mathbf{t}_j^q]$ can be easily restored using the Rodrigues formula in (9) again. With $[d\mathbf{R}_j^q, d\mathbf{t}_j^q]$, the updated rotation matrice $\mathbf{R}_j^q \in SO(3)$ and the updated translation vector $\mathbf{t}_j^q \in \mathbb{R}^3$ in the current q step are computed as that in [2]: $\mathbf{R}_j^q = d\mathbf{R}_j^q\mathbf{R}_j^{q-1}$, $\mathbf{t}_j^q = d\mathbf{R}_j^q\mathbf{t}_j^{q-1} + d\mathbf{t}_j^q$, where $\mathbf{R}_j^{q-1} \in SO(3)$ and $\mathbf{t}_j^q \in \mathbb{R}^{3\times 1}$ are the rotation matrix and translation vector associated with $\mathbf{D}_j$ in the $(q-1)$-th step.

C. M-Cov Step

In this step, we update Σ_j and κ_j for $j = 1,\ldots N$. By solving $\frac{\partial f(\Theta)}{\partial \Sigma_j} = \mathbf{0}_{3\times 3}$ (where $\mathbf{0}_{3\times 3} \in \mathbb{R}^{3\times 3}$ is a zero matrix), we can get the formula of the updated covariance matrix Σ_j^q as:

$$\Sigma_j^q = \frac{\sum_{i=1}^{N_j}\sum_{m=1}^{M}\alpha_{jim}^q\mathbf{z}_{jim}^q(\mathbf{z}_{jim}^q)^{\mathsf{T}}}{N_{\mathbf{P}j}} \tag{12}$$

, where $\mathbf{z}_{jim}^q = \mathbf{x}_{ji} - \mathbf{R}_j^q\mathbf{y}_m - \mathbf{t}_j^q$. Basically, we can see that Σ_j^q is the weighted covariance matrix associated with all the points in the j-th PS and those points in the underlying PS.

Similarly, by solving $\frac{\partial f(\Theta)}{\partial \kappa_j} = 0$ for $j = 1,\ldots N$, we have the equation about κ_j as: $-\frac{1}{\kappa_j} + \frac{e^{\kappa_j}+e^{-\kappa_j}}{e^{\kappa_j}-e^{-\kappa_j}} = \frac{1}{N_{\mathbf{P}j}}\sum_{i=1}^{N_j}\sum_{m=1}^{M}\alpha_{jim}^q(\mathbf{R}_j^q\widehat{\mathbf{y}}_m)^{\mathsf{T}}\widehat{\mathbf{x}}_{ji}$. This non-linear equation of κ_j has no analytical solution, and the fixed-point iteration method is used to solve the problem [60].

D. M-Model Step

In this step, we update the GMMs' means and FMMs' central directions, given the current computed values of $\alpha_{jim}^q, \Sigma_j^q, \kappa_j^q, \mathbf{R}_j^q, \mathbf{t}_j^q$. The GMMs' means are updated by solving $\partial f(\Theta)/\partial\mathbf{y}_m = 0, \forall m \in [1\ldots M]$, which yields the following $\mathbf{y}_m^q = \left(\left(\sum_{ij}\alpha_{jim}^q(\mathbf{x}_{ji}^{\mathsf{T}} - \mathbf{t}_j^{q\mathsf{T}})(\Sigma_j^q)^{-1}\mathbf{R}_j^q\right)\left(\sum_{ij}\alpha_{jim}^q(\mathbf{R}_j^q)^{\mathsf{T}}(\Sigma_j^q)^{-1}(\mathbf{R}_j^q)^{\mathsf{T}}\right)^{-1}\right)^{\mathsf{T}}$. The FMMs' central directions set $\{\widehat{\mathbf{y}}_m\}_{m=1}^M$ are then updated by minimizing $f(\Theta)$ with respect to $\widehat{\mathbf{y}}_m$ subject to the constraints $||\widehat{\mathbf{y}}_m|| = 1, \forall m \in [1\ldots M]$, $\widehat{\mathbf{y}}_m^q = \frac{\sum_{i=1}^{N_j}\sum_{j=1}^{N}\kappa_j^q\alpha_{jim}^q\mathbf{R}_j^{q\mathsf{T}}\widehat{\mathbf{x}}_{ji}}{||\sum_{i=1}^{N_j}\sum_{j=1}^{N}\kappa_j^q\alpha_{jim}^q\mathbf{R}_j^{q\mathsf{T}}\widehat{\mathbf{x}}_{ji}||}$. The above is achieved by constructing and minimizing the Langrangian form of $f(\Theta)$ as $f(\Theta) - \lambda_m(1 - (\widehat{\mathbf{y}}_m)^{\mathsf{T}}\widehat{\mathbf{y}}_m)$ with respect to $\widehat{\mathbf{y}}_m$ for $m = 1,\ldots,M$.

E. Implementation Details

The settings of some parameters involved in the proposed registration algorithm are summarized as follows. The proposed algorithm includes free parameters ω, which is set to be 0.5 because in general do not know the prior of the outliers. The initial value of the positional covariance matrix, in our proposed algorithm, is set as $\Sigma^0 = \text{diag}([100, 100, 100])$. The maximum number of iterations for all test registration method is set to be 100. The initial rotations associated with all point sets, $\{\mathbf{R}_j^0\}_{j=1}^N$ are all set to be the identity matrices $\mathbf{I}_3$. At the same time, the initial translations, $\{\mathbf{t}_j^0\}_{j=1}^N$ are computed as $\mathbf{t}_j^0 = \overline{\mathbf{x}}_j - \mathbf{R}_j^0\overline{\mathbf{y}}^0$, for $j = 1,\ldots,N$, where $\overline{\mathbf{x}}_j$ is the mean position vector of $\mathbf{D}_j$ and $\overline{\mathbf{y}}^0$ is the mean position vector of the initialized central point set $\{\mathbf{y}_m^0\}_{m=1}^M$. The number of components in the central hybrid mixture models, M, is set to be 450.

V. Experiments

To validate the proposed algorithm, two sets of experiments were conducted. In the first experiment, the surface points extracted from a human femur bone model are used. The background of registering multiple point sets together in IGS is the statistical shape modelling (SSM). Fig. 2 shows the four generalized point sets with normal vectors which are represented by arrows. In the second experiment, the surface points extracted from a human pelvis bone model are used. Fig. 6 shows the human pelvis model. The aim of the two experiments is to demonstrate the high registration

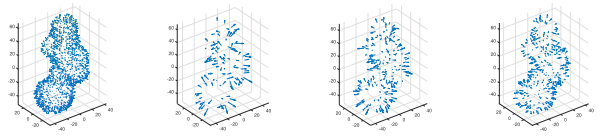

(a) View 1 (b) View 2 (c) View 3 (d) View 4

Fig. 2. The generalized femur bone point sets with normal vectors, which are represented with arrows. The four views of the same human femur bone are (a) view 1 where 1000 inlier points exist. (b) view 2 where 100 inlier points exist. (c) view 3 where 200 inlier points exist. (d) view 4 where 300 inlier points exist. The points in view 2,3 and 4 are plotted before they are disturbed and misaligned.

accuracy, great robustness to noise and outliers of our proposed algorithm by comparing to the state-of-the-art ones. For each case with one specific type of positional noise and one specific percentage of outliers, $N_{trial} = 30$ registration trials have been repeated using the registration algorithms (i.e., ECMPR [36], JRMPC [34], HMM(Iso) [57] and our proposed algorithm). On one hand, we validate the advantage of considering anisotropic positional uncertainty by comparing our method with respect to JRMPC [34] and HMM(Iso) [57] where the assumption of isotropic positional localization error is adopted. On the other hand, we validate the advantage of incorporating the normal vectors by comparing our method with ECMPR [36] and JRMPC [34] where only positional vectors are used in the registration.

To produce corresponding disturbed isotropic normal error vectors, the concentration parameter $\kappa_j = 3200$ ($j = 1, \ldots, N$[1]) in the von-Mises Fisher distribution is used in all the following experiments [58]. The value $\kappa_j = 3200$ actually represents 1° standard deviation in terms of the localization error of the normal vectors. In the first experiment, the number of components in the underlying mixture models, M, is set to be 450 in JRMPC [34], HMM(Iso) [57] and our method. In the second experiment, $M = 600$. On the other hand, the value of the weighting factor w of the outlier distribution in (4) is set to be 0.5 in the two experiments since that we have found that the values of w do not have a significant influence on the registration performances.

VI. Experiments I on Multiple Point Set Registration

In this experiment, four data PSs are jointly registered together. The original model generalized PS $\mathbf{D}_0$ has $N_0 = 1568$ points. Four data generalized PSs $\{\mathbf{D}_j\}_{j=1}^{N}$ ($N = 4$) are first randomly sampled from $\mathbf{D}_0$. Each PS, $\mathbf{D}_j$, has different numbers of generalized points, namely, i.e. $N_1 = 1000$, $N_2 = 100$, $N_3 = 200$ and $N_4 = 300$. Thus, it can be concluded that no exact one-to-one correspondences exist for most of the points in each two PSs. The three observed PSs $\{\mathbf{D}_j\}_{j=2}^{4}$ are further misaligned to own inherent transformation matrices $\{\mathbf{R}_{true,j}, \mathbf{t}_{true,j}\}_{j=2}^{4}$ with respect to the first PS $\mathbf{D}_1$. For simplicity, we sometimes refer to one PS as one 'view' hereafter. The 'true' misalignments $\{\mathbf{R}_{true,j}, \mathbf{t}_{true,j}\}_{j=2}^{4}$ are randomly and uniformly sampled in $[0, 10]^\circ$ and $[0, 10]$ mm. Moreover, position-al noise, orientation-al noise and outliers are further injected to produce the four misaligned observed PSs. Nine cases with different percentages of outliers are adopted: 10% to 90% with 10% interval. Our aim is to register all the four misaligned observed PSs $\{\mathbf{D}_j\}_{j=1}^{4}$ together (i.e., to find the rigid transformations between each two PSs). The rotational error value (in degree) denoted as $\theta_{err,j}^{k}$ associated with the j-th PS in the k-th registration trial is formally defined as the following:

$$\theta_{err,j}^{k} = \arccos\left[\frac{\mathrm{tr}(\mathbf{R}_{true,j}^{k}(\widehat{\mathbf{R}}_{cal,j}^{k})^{\mathsf{T}} - 1)}{2}\right] \times 180/\pi \ , \quad (13)$$

With the ECMPR method [36], $\{\widehat{\mathbf{R}}_{cal,j}^{k}\}_{j=2}^{4}$ is calculated by registering the disturbed misaligned observed PSs $\{\mathbf{D}_j\}_{j=2}^{4}$ to $\mathbf{D}_1$ respectively. With JRMPC [34], HMM(Iso) [57] and our method, the estimated rotation matrix $\widehat{\mathbf{R}}_{cal,j}^{k}$ associated with the j-th PS (i.e. $\mathbf{D}_j$) is computed as $(\widehat{\mathbf{R}}_1^k)^{\mathsf{T}}\widehat{\mathbf{R}}_j^k$, where $\{\widehat{\mathbf{R}}_j^k\}_{j=2}^{4}$ are the computed rotation matrices that align $\{\mathbf{D}_j\}_{j=2}^{4}$ with the underlying model PS in the k-th registration trial. In the registration process using JRMPC [34], HMM(Iso) [57] and our algorithm, all the PSs are registered together and no PS is considered as the referenced one. In the evaluation process, we should note that it makes no difference which PS serves as the reference one. For convienience, we use the first PS as the reference one when we evaluate the three registration algorithms.

A. Isotropic/Anisotropic Positional Noise

In the case of isotropic positional noise, the noise vectors generated with covariance matrices $\Sigma_j^{injected}{}^2 = \frac{1}{3}\mathbf{I}_3$ (where $j = 1, \ldots 4$) is injected into $\{\mathbf{D}_j\}_{j=1}^{4}$. In the case of anisotropic positional noise, noise vectors generated from the covariance matrices $\Sigma_j = \mathrm{diag}([1/11, 1/11, 9/11])$(where$j = 1, \ldots 4$) are injected into $\{\mathbf{D}_j\}_{j=1}^{4}$. The larger value along the z-axis in Σ_j is realistic since that in a stereo-camera, the localization error's variance in the viewing direction of the camera is 3-5 times of those in the other two directions.

We plot the mean rotational error values[3] associated with the view 2, 3, and 4 in Fig. (3) in cases of isotropic and anisotropic positional noise. Fig. 3 (a) shows that (1) in the case of isotropic positional noise, the proposed method outperforms ECMPR [36] and JRMPC [34] methods with a large margin, which demonstrates the advantage of incorporating the normal vectors into the registration process. (2) HMM(Iso) and the

[1] N represents the number of PSs to be registered. In the first experiment, $N = 4$. In the second experiment, $N = 2$.

[2] Note that $\Sigma_j^{injected}$ is in the coordinate system of $\mathbf{D}_j$, where $j = 1, \ldots, N$. Let $\mathbf{R}_{true,j}$ be the ground-truth rotation matrix that align the model PS $\{\mathbf{d}_m\}_{m=1}^{M}$ to $\mathbf{D}_j$. Then a noise vector $\mathbf{v}$ randomly sampled from a zero-mean Gaussian distribution with the covariance matrix being $\Sigma_j^{injected}$ is added to the noise-free model point $\mathbf{R}_{true,j}\mathbf{y}_m$. That disturbed positional vector is denoted as $\mathbf{R}_{true,j}\mathbf{y}_m + \mathbf{v}$, which can also be written as $\mathbf{R}_{true,j}(\mathbf{y}_m + \mathbf{R}_{true,j}^{\mathsf{T}}\mathbf{v})$. In other words, the injected noise to $\mathbf{y}_m$ is draw from a zero-mean Gaussian distribution with the covariance matrix being $\mathbf{R}_{true,j}^{\mathsf{T}}\Sigma_j^{injected}\mathbf{R}_{true,j}$, whose non-diagonal elments are not-zero.

[3] For example, in one specific test case, the mean rotational error value (in degree) associated views 2,3 and 4 is computed as: $\frac{\sum_{j=1}^{3}\sum_{k=1}^{N_{trial}}\theta_{err,j}^{k}}{3N_{trial}}$, where $\theta_{err,j}^{k}$ is computed using (13).

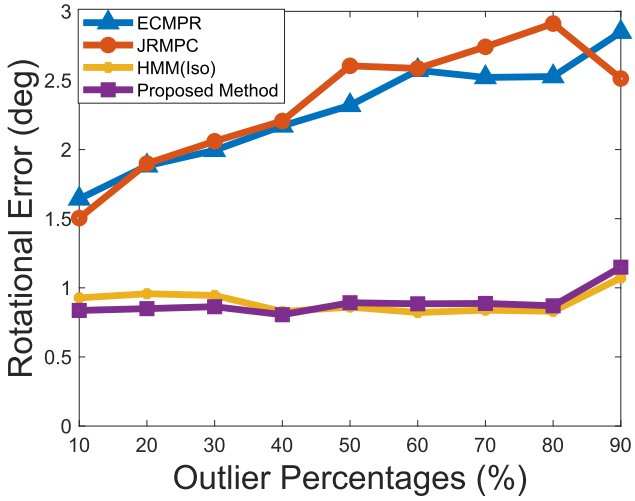

(a) Isotropic noise

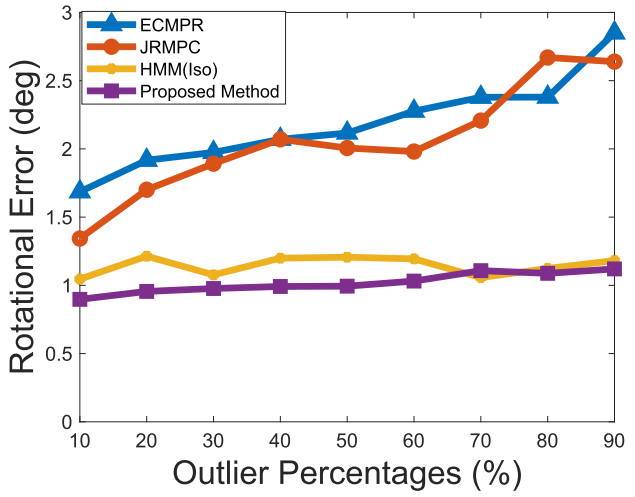

(b) Anisotropic noise

Fig. 3. The mean rotational error value in degree of N_{trial} registration trials associated with the view 2, view 3 and view 4 using ECMPR [36], JRMPC [34], HMM (Iso) [34] and our proposed method in all test cases. A specific percentage of outliers is used in each test case. The results are of the cases (a) isotropic positional noise is injected into four PSs; (b) anisotropic noise is injected into four PSs.

proposed method's performances are close. Fig. 3 (b) shows that (1) in the case of anisotropic positional noise, the proposed method also outperforms ECMPR [36] and JRMPC [34] methods with a large margin. (2) the proposed method outperforms HMM(Iso) in cases of 10%-60% outliers.

B. Influence of the Weighting Factor w on the Registration Accuracy

The weighting factor of the outlier distribution w in (4) is one user-specified hyper-parameter in our algorithm. The influence of w on the registration's performance (i.e. accuracy) is explored in this section. We vary the values of w in (4) in the range [0.1, 0.9] with the interval being 0.1, where 30% outliers and anisotropic noise are injected into $\{\mathbf{D}_j\}_{j=1}^4$. In this series of experiments, M is set to be 450. For each test case

TABLE I

THE P-VALUES OF THE STATISTICAL TESTS COMPARING THE N_{trial} ROTATIONAL ERROR VALUES (IN DEGREE) WHEN $w = 0.1$ WITH THOSE WHEN $w = 0.2, \ldots, 0.9$ FOR THE LATER THREE VIEWS, RESPECTIVELY. IN THIS SERIES OF EXPERIMENTS, ANISOTROPIC POSITIONAL NOISE AND 30% OUTLIERS ARE INJECTED IN THE FOUR POINT SETS (I.E. VIEWS). THE VALUE OF M IS SET TO BE 450

w	0.2	0.3	0.4	0.5	0.6	0.7	0.8	0.9
View 2	0.4822	0.7948	0.5288	0.7893	0.9744	0.9830	0.7015	0.1765
View 3	0.1412	0.7547	0.1260	0.3512	0.6578	0.5172	**0.0486**	0.8566
View 4	**0.0254**	0.2291	**0.0093**	0.3654	0.2656	0.5211	0.0752	0.3863

with a specific w, $N_r = 10$ registration trials are repeated. Fig. 4 (a) shows the mean of the N_r rotational error values (in degree) associated with the three views with different values of w. As can be seen from Fig. 4 (a), the mean rotational error values are stable with different w.

Paired-sampled t-tests ($\alpha = 0.05$) are conducted comparing the N_r rotational error values associated with the three views when $w = 0.1$ and the N_r rotational error values when $w = 0.2, \ldots, 0.9$, respectively. In all, we get $3 \times 8 = 24$ p-values that are summarized in Table I. To summarize, 21 out of 24 (87.5%) cases do not pass the statistical tests. In other words, the choice of w does not influence the final rotational error values significantly in most cases.

C. Influence of the Number of Central Model's Components M on the Registration Accuracy

The number of components M in HMMs (or equally the number of points in the model point set) is another important user-specified hyperparameter that may influence the algorithm's performances. In this section, we vary M from 200 ($\frac{\sum_{j=1}^N N_j}{2N}$) to 600 ($\frac{3\sum_{j=1}^N N_j}{2N}$) with the interval being 50, where at the same time the anisotropic positional noise and 30% outliers are injected into $\{\mathbf{D}_j\}_{j=1}^4$. The parameter w is set to be 0.5. For each test case with a specific value of M, $N_r = 10$ registration trials are repeated. Fig. 4 (b) shows the mean of the N_{trial} rotational error values (in degree) associated with the three views with different M. In Fig. 4 (b), we denote the cases with $M = 200, \ldots, 600$ as case 1 to case 9 respectively. As can be seen from Fig. 4 (b), the mean rotational error values slightly decreases with larger M.

To formally see if there are statistically significant differences between results with different M, we conduct the paired-sampled t-test ($\alpha = 0.05$ level) using the recorded error values associated with the three views (between those with $M = 200$ and those with $M \neq 200$), respectively. In all, we get $3 \times 8 = 24$ p-values that are summarized in Table. II. The p-values that are smaller than 0.05 are emphasized using black bold, which indicates that the error differences are statistically meaningful for those cases. As shown in Table. II, (1) seven out of 24 cases (i.e., 29.17%) demonstrates statistically significant differences. (2) most of the test cases (70.83%) shows no significant differences between different M. As discussed in [34], the value of M can be safely chosen from the range $[\frac{\sum_{j=1}^N N_j}{2N}, \frac{3\sum_{j=1}^N N_j}{2N}]$.

TABLE II

THE P-VALUES OF THE 24 PAIRED-T TESTS COMPARING THE RECORDED ROTATIONAL ERROR VALUES WHEN $M = 200$ WITH THOSE WHEN $M = 250, \ldots, 600$ FOR THE LATER THREE VIEWS, RESPECTIVELY. IN THIS SERIES OF EXPERIMENTS, ANISOTROPIC NOISE AND 30% OUTLIERS ARE INJECTED IN THE FOUR POINT SETS (I.E. VIEWS). THE WEIGHTING VARIABLE w IS SET TO BE 0.5

M	250	300	350	400	450	500	550	600
View 2	0.3712	0.8702	0.6092	0.8047	0.6638	0.4134	0.2599	0.1720
View 3	0.1508	0.9069	0.9579	0.3507	0.3664	0.4608	0.3055	0.1538
View 4	0.4674	**0.0069**	**0.0136**	**0.0114**	$\mathbf{3.1077 \times 10^{-4}}$	**0.0013**	$\mathbf{2.6539 \times 10^{-4}}$	$\mathbf{3.4373 \times 10^{-4}}$

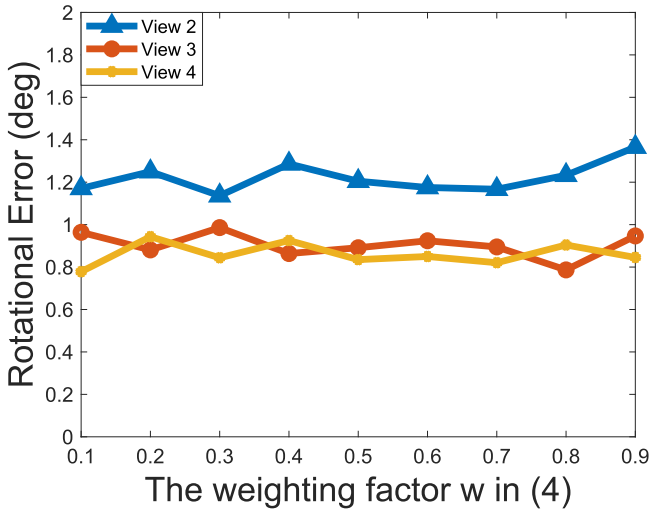

(a) Effect of the weight w

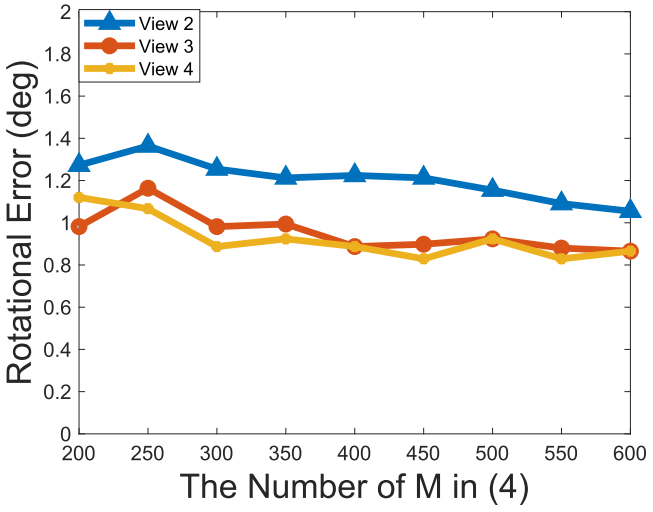

(b) Effect of M

Fig. 4. (a) The effect of the weighting factor w in (4) on the rotational error in degree, when anisotropic positional noise and 30% outliers are injected into the four PSs. (b) The effect of the number of components M in (4) on the rotational error in degree, when anisotropic positional noise and 30% outliers are injected into the four PSs.

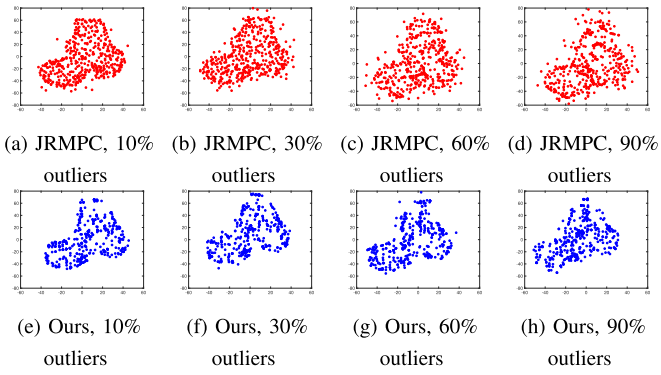

(a) JRMPC, 10% outliers (b) JRMPC, 30% outliers (c) JRMPC, 60% outliers (d) JRMPC, 90% outliers

(e) Ours, 10% outliers (f) Ours, 30% outliers (g) Ours, 60% outliers (h) Ours, 90% outliers

Fig. 5. The integrated model point set recovered using (a-d) JRMPC method, (e-h) our method with different percentages of outliers injected into the point sets.

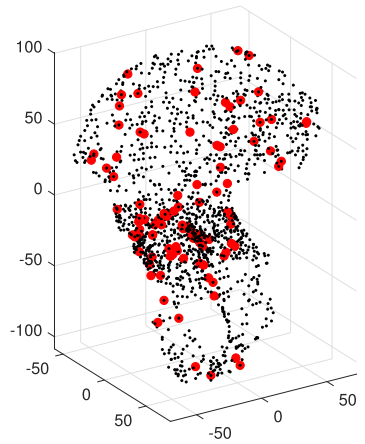

Fig. 6. The pelvis (hip) point set used in the Experiment II in Section. VII. The black dots represent the model point set while the red dots denote the sampled points from the model point set (before they are futher disturbed and misaligned).

D. Integrated Model

Both JRMPC method and our algorithm can recover the underlying 'noise-free' model PS. We compare the recovery abilities using both algorithms. Fig. 5 (a-d) and (e-f) show the recovered integrated PS using the JRMPC method and our algorithm with i) different percentages of outliers; ii) anisotropic noise injected into all observed PSs. As can be seen from Fig. 5, in all test cases, our algorithm is able to recover the model PS with (i) a much smoother boundary and (ii) fewer outliers than the JRMPC method is. By comparing Fig. 5 (a-d) with (e-f), we can also see that the integrated model with our algorithm is more robust to outliers.

VII. EXPERIMENTS II ON PAIR-WISE POINT SET REGISTRATION

In computer-assisted orthopedic surgery (CAOS), the pre-operative surgical plan is tailored in the volumetric medical

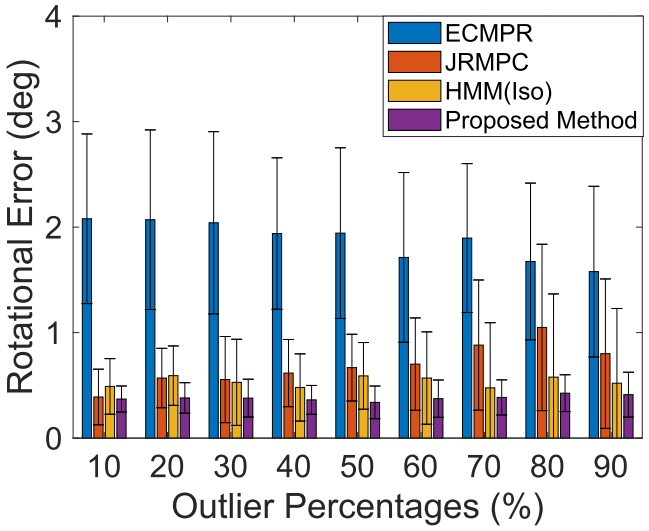

(a) isotropic position noise

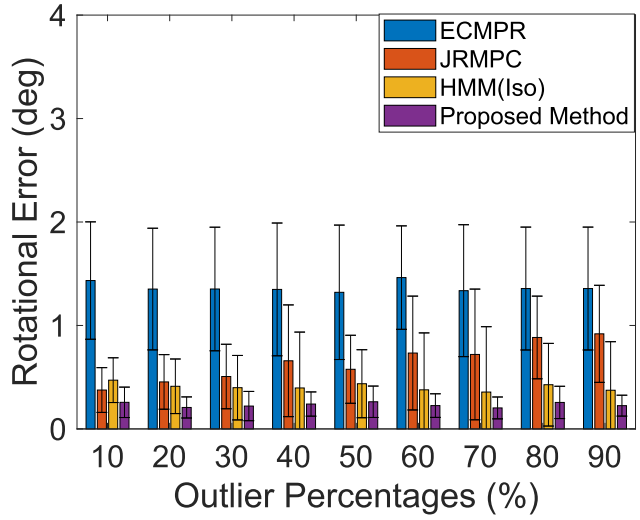

(b) anisotropic position noise

Fig. 7. Summarized statistics include the mean and standard deviation of the N_{trial} rotational error values in degree in each test case where a specific percentage of outliers is used. The results are (a) isotropic positional noise; (b) anisotropic positional noise.

images (e.g., CT images) while the actual surgical operation is conducted in the patient coordinate frame. To utilize the pre-operative planning information, the pre-operative space has to be registered with the intra-operative space in order to provide accurate surgical guidance to the surgeon or medical robot during surgery. Compared to the PSs segmented from the pre-operative images, the intra-operative PSs usually have much fewer points. As shown in Fig. 6, the intra-operative points (in red) are sampled from the pre-operative PSs (in black). In this experiment, we conduct the experiments on the PS representing the human pelvis bone. We are registering two PSs in this experiment. The model pelvis PS $\mathbf{D}_0$ has $N_0 = 1568$ generalized points. In each registration trial, the 'true' misalignment $[\mathbf{R}_{true}, \mathbf{t}_{true}]$ is randomly sampled from $[10, 20]^\circ$ and $[10, 20]$ mm, and applied to the model PS $\mathbf{D}_0$. $\mathbf{D}_0$ is then misaligned to create the mis-aligned $\mathbf{D}_0$. The $N_1 = 100$ points in the data point set (i.e., $\mathbf{D}_1$) are randomly

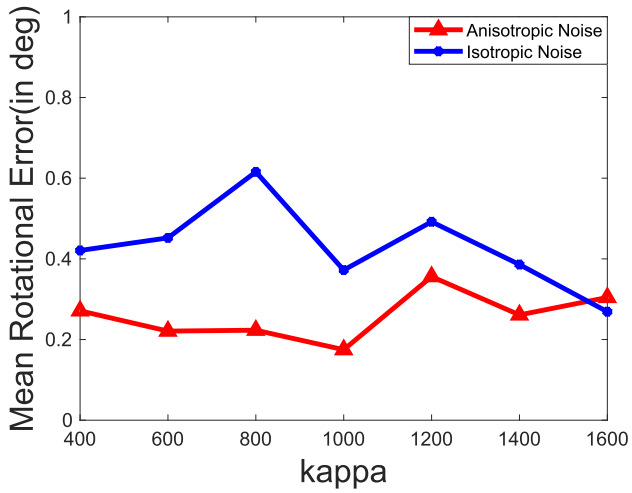

Fig. 8. The mean rotational error values in degree with respect to the different values of kappa. The readers should note that smaller values of κ correspond to larger orientational error values.

sampled from $\mathbf{D}_0$ and disturbed with Gaussian positional noise and orientation-al noise, respectively. As is in the case of registering multiple PSs: (i) The isotropic covariance matrix Σ is $\Sigma = \frac{1}{3}\mathbf{I}_3$, (ii) The anisotropic covariance matrix Σ is $\Sigma = \text{diag}([1/11, 1/11, 9/11])$. In addition, nine cases of different percentages of outliers are injected into the $\mathbf{D}_1$: 10% to 90%. More specifically, for example, 10 outlier generalized points exist in $\mathbf{D}_1$ when 10% outliers are injected. In this experiment, we are registering the misaligned $\mathbf{D}_0$ with $\mathbf{D}_1$. The rotational error value (in degree) is defined as the following: $\theta^k_{err} = \arccos\left[\frac{\text{tr}(\mathbf{R}^k_{true}(\widehat{\mathbf{R}}^k_{cal})^\mathsf{T}-1)}{2}\right] \times 180/\pi$,, where $\widehat{\mathbf{R}}^k_{cal}$ is the estimated rotation matrix in the k-th registration trial using the ECMPR [36], JRMPC [34], HMM(Iso) [57] and our proposed algorithm. The computation procedures of $\widehat{\mathbf{R}}^k_{cal}$ using the above four registration algorithms are similar to those described in the first experiment. The number of points in the underlying model PS (i.e. M) is set to be 600 in this experiment. The weighting factor w of the outlier distribution in (4) is set to be 0.5.

Fig. 7 shows the mean and standard deviation of the $N_{trial} = 30$ rotational error values for each test case, under both isotropic and anisotropic positional noise. As shown in Fig. 7, our proposed algorithm outperforms ECMPR [36], JRMPC [34], and HMM(Iso) [57] in all test groups and is very robust to additional injected outliers.

A. Influence of κ

In this section, we explore the influence of κ (i.e., the localization error magnitudes associated with the normal vectors) on the performances of our proposed method. As it can be seen from Fig. 8, there is no evident increase of the rotational error values with larger injected orientational error (i.e. smaller values of κ) in both cases of anisotropic (in blue) and isotropic (in red) positional noise. We further conduct statistical analysis to verify if there is a statistical difference between the rotational error values with respect to different

TABLE III
THE REGISTRATION ERROR VALUES WITH THE ALGORITHM'S ITERATIONS

Iteration 0	Iteration 1	Iteration 5	Iteration 10	Iteration 12
13.7265°	6.9963°	0.5747°	0.4751°	0.1313 °
24.4170mm	2.1177mm	1.1293mm	0.2751 mm	0.0787 mm

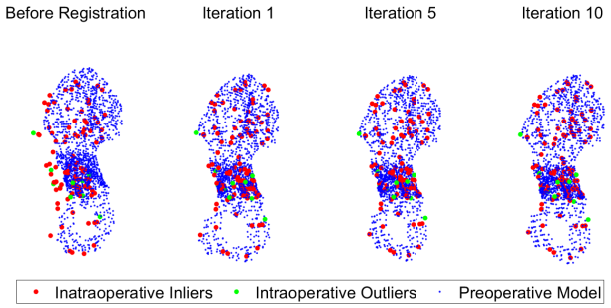

Fig. 9. The qualitative results of the registration process on the human pelvis model point sets. The red, yellow and blue dots denote the intra-operative inlier, intra-operative outliers, and the pre-operative model points, respectively. As can be seen from left to right, the red and blue points will become closer and closer in the 3D space, which indicates the two point sets are registered aggressively.

values of κ. We compare the results where $\kappa = 1600$ with those where $\kappa = 400$, $\kappa = 600$, $\kappa = 800$, $\kappa = 1000$, $\kappa = 1200$ and $\kappa = 1400$ respectively, in both cases of anisotropic and isotropic positional noise. We found that most κ values are larger than 0.05, which means that the results are not statistically different at the significant level $\alpha = 0.05$. Only one case that the p-value is smaller than 0.05. We thus conclude that our proposed approach is thus very robust to the increasing error values associated with the normal vectors.

B. Qualitative Results in the Registration Process

In this section, we include the registration processes with both quantitative and qualitative results. Fig. 9 shows the qualitative results. By looking carefully into this plot, the readers can see that the red points (intra-operative points) can well align with the blue points (pre-operative points) after the iteration 10. Table. III includes the corresponding quantitative results, which include the rotational and translational error values. As can be seen from Table. III, both the rotational and translational error values decrease to a very low level(i.e. 0.5747° and 1.1293mm respectively) after **five** iterations.

VIII. DISCUSSION

Accurately aligning multiple PSs into one common coordinate frame is the first and also essential step in statistical shape modelling (SSM). In this paper, we have proposed a novel probabilistic approach to jointly register multiple generalized PSs. The core idea is to consider that the generalized PSs are generated by an underlying unknown hybrid mixture model (HMM). The unknown model PS can be recovered at the end of our approach. We have demonstrated through experiments that in cases of both isotropic and anisotropic positional noise, our algorithm (i) achieves lower registration error; (ii) is more robust to outliers. We have also found that the weight of the additional uniform distribution in our model will not affect the algorithm's performance in a statistically significant manner.

Varying percentages of outliers commonly exist in shapes extracted from volumetric medical images [26]. Experimental results show that our algorithm owns great robustness to large injected outliers. Compared with other registration methods, our algorithm shows significant improvement when the PS is sparse (i.e., the 'View 2' in our case). The robustness to outliers of our algorithm partially benefits from the utilization of normal vectors.

Our algorithm treats all PSs equally and thus there is no bias towards one specific PS. Our algorithm significantly improves the JRMPC method in the following two aspects. First, the normal vectors associated with each point are used. Second, the position localization error is assumed to obey multi-variate Gaussian distributions to accommodate anisotropic noise in the scenario of surgical navigation. With the assumption of anisotropic positional noise, computing the rigid transformation parameters does not have a closed-form solution, which led us to reformulate the associated non-convex optimization problems of updating the rigid transformation matrices into unconstrained convex ones. To speed up the optimization process, we compute and present the gradients of the objective function to be minimized.

Another advantage/byproduct of jointly registering multiple point sets is that the central model PS can be acquired after the registration procedure. To note, both JRMPC and our algorithm can recover the unknown central model PS. Compared to the JRMPC method, our algorithm is able to recover a model PS in a more accurate way and is also more robust to outliers. Our work has several limitations. First, all the theoretical derivations of this article are based on the assumption that the positional and normal vectors are independent, which is a very strong assumption and maynot be correct in all practical situations. Second, the proposed algorithm has some user-specified parameters including (i) the weight of the uniform distribution w in the overall PDF; (ii) the number of points M in the underlying model PS. Although we have experimentally verified that the above two parameters do not influence much the final registration accuracy, the verifications are only done on limited data sets. Third, the proposed algorithm may not very suitable to large scale point sets, which can consume a lot of computational time and may make the optimization problem intractable. Fourth, we only test our algorithm on the bone data sets which are convex. The interested readers can further apply the algorithm on other medical data sets that are more complex. Fifth, the PSs used in both experiments are from one same human subject. Future work includes extending/modifying the proposed algorithm to registering the models from multiple subjects.

IX. CONCLUSION

In this article, we have presented a novel probabilistic method to jointly register multiple generalized PSs considering anisotropic positional uncertainties. The core idea is to regard all the generalized PSs as the transformed realizations of underlying unknown hybrid mixture models (HMMs).

We have demonstrated through extensive experiments that our algorithm; (i) achieves significant lower registration error values; (ii) is more robust to outliers (iii) converges much faster than the state-of-the-art registration methods. The results show both theoretical and clinical value of our proposed method.

APPENDIX A
NOMENCLATURE

This article has the following notation conventions:

- $N \in \mathbb{R}$ - the number of observed generalized point sets to be registered,
- $j \in \mathbb{R}$ - the index of one observed generalized point set,
- $\mathbf{D}_j$ - the j-th observed generalized point set,
- $\mathbf{D}$ - the union set of all the observed generalized point set,
- $i \in \mathbb{R}$ - the index of one generalized point in $\mathbf{D}_j$,
- $N_j \in \mathbb{R}$ - the number of generalized points in $\mathbf{D}_j$,
- $M \in \mathbb{R}$ - the number of generalized points in the underlying model point set,
- $q \in \mathbb{R}$ - the index of the registration algorithm's iteration,
- N_{trial} - the number of trials conducted in each test case,
- $\mathbf{d}_{ji} \in \mathbb{R}^{6\times 1}$ - the i-th generalized point in $\mathbf{D}_j$,
- $m \in \mathbb{R}$ - the index of one generalized point in the underlying model point set,
- $\mathbf{d}_m \in \mathbb{R}^{6\times 1}$- the m-th generalized point in the underlying model point set,
- $\mathbf{R}_j \in SO(3)$ - the rotation matrix that aligns the underlying model point set with $\mathbf{D}_j$,
- $\mathbf{t}_j \in \mathbb{R}^{3\times 1}$ - the translational vector that aligns the underlying model point set with $\mathbf{D}_j$
- $\kappa_j \in \mathbb{R}$ - the concentration parameter of the von-Mises-Fisher (VMF) distribution for orientation-al uncertainty associated with $\mathbf{D}_j$,
- $\Sigma_j \in \mathbb{S}^{3\times 3}$ - the positional covariance matrix associated with $\mathbf{D}_j$,
- $\mathbf{A}^{\mathsf{T}}$ - the transpose of a vector or a matrix $\mathbf{A}$,
- Θ_{jrmpc}- the model parameters used in the joint registration of multiple point clouds (JRMPC) method $\Theta_{jrmpc} = \{\{\mathbf{R}_j, \mathbf{t}_j\}_{j=1}^{N}, \{\mathbf{y}_m, \sigma_m\}_{m=1}^{M})\}$
- Θ - the model parameters in our proposed algorithm $\Theta = (\{\mathbf{R}_j, \mathbf{t}_j, \kappa_j, \Sigma_j\}_{j=1}^{N}, \{\mathbf{d}_m\}_{m=1}^{M})$,
- Θ^q - the model parameters in the q-th step $(\{\mathbf{R}_j^q, \mathbf{t}_j, \kappa_j, \Sigma_j\}_{j=1}^{N}, \{\mathbf{d}_m\}_{m=1}^{M})$
- $P(z_{ji} = m)$ - the prior correspondence probability,
- Θ_p - model parameters of positional data $\{\mathbf{R}, \mathbf{t}, \sigma^2\}$,
- Θ_o - model parameters of orientational data $\{\mathbf{R}, \kappa\}$,
- $z_{ji} \in \{z_{ji} \in \mathbb{Z}, 1 \le z_{ji} \le M+1\}$ - the correspondence variable,
- $\mathbf{1}$ - a vector with all elements being one,
- $\mathbf{I}_{3\times 3}$ - the identity matrix of dimension 3,
- $\mathrm{Tr}(\bullet)$ - trace of a matrix,
- $\mathrm{diag}(\bullet)$ - diagonal matrix of a vector,
- $\det(\bullet)$ - determinant of a matrix,
- $||\bullet||_F$ - Frobenius norm of a matrix,
- $\alpha_{jim} \in \mathbb{R}$ - the posterior probability that assigns $\mathbf{d}_{ji}$ to the m-th point in the underlying model point set,
- $w \in \mathbb{R}$ - the weight of the inliers in the mixture models,
- GMM - Gaussian mixture model,
- FMM - Fisher mixture model,
- HMM - Hybrid mixture model.

APPENDIX B
VON-MISES FISHER DISTRIBUTION

In this section, we briefly introduce the basics of von-Mises-Fisher (vMF) distribution that is used to model the orientation-al error [58]. The probability density function of the vMF distribution for the random d-dimensional unit vector $\widehat{\mathbf{x}}$ (i.e. $\widehat{\mathbf{x}} \in \mathbb{R}^d$ and $||\widehat{\mathbf{x}}|| = 1$, or equivalently $\widehat{\mathbf{x}} \in \mathbb{S}^{d-1}$) is given by $p(\widehat{\mathbf{x}}|\widehat{\boldsymbol{\mu}}, \kappa) = c_d(\kappa)e^{\kappa\widehat{\boldsymbol{\mu}}^{\mathsf{T}}\widehat{\mathbf{x}}}$, where $||\widehat{\boldsymbol{\mu}}|| = 1, \kappa \ge 0$ and $d \ge 2$. The normalizing constant $c_d(\kappa)$ is $c_d(\kappa) = \frac{\kappa^{d/2-1}}{(2\pi)^{d/2} I_{d/2-1}(\kappa)}$, where $I_r(\bullet)$ denotes the modified Bessel function of the first kind and order r. The above density function $p(\widehat{\mathbf{x}}|\widehat{\boldsymbol{\mu}}, \kappa)$ is parameterized by the mean direction $\widehat{\boldsymbol{\mu}}$ and the concentration parameter κ. We remark that larger values of κ indicate stronger concentration about the mean direction. More specifically, in our case (where $d = 3$), the normalizing constant $c_d(\kappa)$ is the following: $c_d(\kappa) = \frac{\kappa}{2\pi(e^{\kappa} - e^{-\kappa})}$.

APPENDIX C
A BRIEF INTRODUCTION OF THE JRMPC ALGORITHM

In this section, we give a brief discussion of the joint registration of multiple point clouds (JRMPC) algorithm. The idea of the JRMPC method is to regard all the PSs to be registered as the samples of the transformed central PSs. In JRMPC, each point in the central PS owns a specific standard deviation σ_m. Then we could have the probability density function of an observed point $\mathbf{x}_{ji}$, given the correspondence $z_{ji} = m$ and the model parameters $\Theta_{jrmpc} = \{\{\mathbf{R}_j, \mathbf{t}_j\}_{j=1}^{N}, \{\mathbf{y}_m, \sigma_m\}_{m=1}^{M})\}$ as follows

$$p(\mathbf{x}_{ji}|z_{ji} = m, \Theta_{jrmpc}) = \frac{1}{(2\pi\sigma_m^2)^{\frac{3}{2}}} e^{-\frac{1}{2\sigma_m^2}||\mathbf{x}_{ji} - \mathbf{R}\mathbf{y}_m - \mathbf{t}||^2} \quad (14)$$

Given the independence between the observed points, we can have the complete PDF of an observed point as follows

$$p(\mathbf{x}_{ji}|\Theta_{jrmpc}) = \sum_{m=1}^{M} p_m\, p(\mathbf{x}_{ji}|z_{ji} = m, \Theta_{jrmpc}) + p_{M+1}\mathcal{U}(h) \quad (15)$$

where p_m and p_{M+1} are the mixing coefficients of the Gaussian mixtures and the additional uniform distribution $\mathcal{U}(h)$ which is used to account for the outliers, where $h \in \mathbb{R}$ represents the volume. The joint probability density function is

$$p(\mathbf{X}, \mathcal{Z}|\Theta_{jrmpc}) = \prod_{ji} p(\mathbf{x}_{ji}|z_{ji}, \Theta_{jrmpc}), \quad (16)$$

To find the optimal estimation of Θ is to minimize the expected *negative log-likelihood* term with respect to the latent variables $\mathcal{Z}$,

$$\begin{aligned} Q(\Theta_{jrmpc}|\mathbf{X}, \mathcal{Z}) &= \mathbb{E}_{\mathcal{Z}}[\log p(\mathbf{x}, \mathcal{Z}|\Theta_{jrmpc}] \\ &= \sum_{\mathcal{Z}} P(\mathcal{Z}|\mathbf{X}, \Theta_{jrmpc}) \log\big(p(\mathbf{X}, \mathcal{Z}; \Theta_{jrmpc})\big) \end{aligned} \quad (17)$$

Although in their derivations, the covariance matrix Σ_m is used, we find that in both the expectation and maximization steps the isotropic assumption is still used. Assuming that the observed data are independent and identical distributed, the objective function is written as the following:

$$\begin{aligned} &Q(\Theta_{jrmpc}) \\ &= -\frac{1}{2}\sum_{jim}\alpha_{jim}\Big(||\mathbf{x}_{ji}-\mathbf{R}_j\mathbf{y}_m-\mathbf{t}_j||^2+\frac{3}{2}\log\sigma_m^2-2\log p_m\Big) \\ &\quad+\log p_{M+1}\sum_{ji}\alpha_{ji(M+1)} \end{aligned} \tag{18}$$

In order to acquire Θ_{jrmpc} by minimizing $Q(\Theta_{jrmpc})$, the expectation maximization technique is used. In the expectation step, the posteriors α_{jim} are computed given the current rigid transformation matrices. In the maximization steps, given the current posteriors, the rigid transformation matrices $\{\mathbf{R}_j,\mathbf{t}_j\}_{j=1}^N$, the central PSs $\{\mathbf{y}_m\}_{m=1}^M$ together with their associated standard deviation values $\{\sigma_m^2\}_{m=1}^M$ are updated in a sequential manner. The expectation and maximization steps will iterate until convergence.

The main differences and improvements of our proposed algorithm with respect to the original JRMPC method are summarized as follows. First, we have generalized the original JRMPC algorithm to the six-dimensional PSs. Normal vectors that are used can be thought of as first-order features, which can be extracted from the PSs. With more enrich information used, we would like to enhance the registration's robustness and accuracy. Second, we have generalized the assumption of isotropic Gaussian distribution associated with the positional error to anisotropic one. Third, each mixture model component owns its distinctive parameters σ_m in the JRMPC method. On the other hand, as will introduced in our method, each point set owns its specific parameters Σ_j and κ_j. The insight of formulating the mixture models in this way is that the multiple PSs may come from different modalities, and thus may own different measurement uncertainties. We have compared the registration performances using the above two formulations and found that the current formulation works better.

APPENDIX D
WHEN Σ_j IS A DIAGONAL MATRIX

A. The Simplified Probability Density Function (PDF)

Let $\Sigma_\mathbf{j}$ be a diagonal covariance matrix denoted as

$$\Sigma_j=\begin{bmatrix}\sigma_x^2&0&0\\0&\sigma_y^2&0\\0&0&\sigma_z^2\end{bmatrix} \tag{19}$$

Then we can easily get the determinant of the $|\Sigma_j|=\sigma_x^2\sigma_y^2\sigma_z^2$, $|\Sigma_\mathbf{j}|^{\frac{1}{2}}=\sigma_x\sigma_y\sigma_z$ and

$$\mathbf{z}_{jim}^\mathsf{T}\Sigma_j^{-1}\mathbf{z}_{jim}=\mathbf{z}_{jim}^\mathsf{T}\begin{bmatrix}\frac{1}{\sigma_x^2}&0&0\\0&\frac{1}{\sigma_y^2}&0\\0&0&\frac{1}{\sigma_z^2}\end{bmatrix}\mathbf{z}_{jim}=\mathbf{z}_{jim}^\mathsf{T}\mathbf{z}_{jim}^{weighted}.$$

With the above expression, we can get the simplied version of PDF in (3) as follows,

$$\begin{aligned} &p(\mathbf{d}_{ji}|z_{ji}=m,\Theta_{jm}) \\ &=\underbrace{\frac{1}{(2\pi)^{\frac{3}{2}}|\Sigma_j|^{\frac{1}{2}}}e^{\frac{-1}{2}\mathbf{z}_{jim}^\mathsf{T}\mathbf{z}_{jim}^{weighted}}}_{Gaussian}\underbrace{\frac{\kappa_j}{2\pi(e^{\kappa_j}-e^{-\kappa_j})}e^{\kappa_j(\mathbf{R}_j\widehat{\mathbf{y}}_m)^\mathsf{T}\widehat{\mathbf{x}}_{ji}}}_{Fisher} \\ &=\frac{\kappa_j}{(2\pi)^{\frac{5}{2}}\sigma_x\sigma_y\sigma_z(e^{\kappa_j}-e^{-\kappa_j})}e^{\kappa_j(\mathbf{R}\widehat{\mathbf{y}}_m)^\mathsf{T}\widehat{\mathbf{x}}_{ji}-\frac{1}{2}(\mathbf{z}_{jim}))^\mathsf{T}\Sigma_j^{-1}(\mathbf{z}_{jim})} \end{aligned} \tag{20}$$

The simplified version of (4) can be derived from the above expression.

B. The Simplified Objective Function $\mathbf{C}_{P,jim}$ in (8)

The $\mathbf{C}_{P,jim}$ in (8) is rewritten as follows,

$$\begin{aligned} &\frac{1}{2}\alpha_{jim}^q(\mathbf{z}_{jim}^q)^\mathsf{T}\Sigma_j^{-1}\mathbf{z}_{jim}^q \\ &\quad=\frac{1}{2}\alpha_{jim}^q(\mathbf{z}_{jim}^q)^\mathsf{T}\begin{bmatrix}\frac{1}{\sigma_x^2}&0&0\\0&\frac{1}{\sigma_y^2}&0\\0&0&\frac{1}{\sigma_z^2}\end{bmatrix}\mathbf{z}_{jim}^q \end{aligned} \tag{21}$$

Let the definition of d be the follows,

$$\mathbf{z}_{jim}^q=\begin{bmatrix}(\mathbf{z}_{jim}^q)_x\\(\mathbf{z}_{jim}^q)_y\\(\mathbf{z}_{jim}^q)_z\end{bmatrix} \tag{22}$$

The expression of $\frac{1}{2}\alpha_{jim}^q(\mathbf{z}_{jim}^q)^\mathsf{T}\Sigma_j^{-1}\mathbf{z}_{jim}^q$ is reduced to

$$\mathbf{C}_{P,jim}=\frac{1}{2}\alpha_{jim}^q\Big(\frac{1}{\sigma_x^2}(\mathbf{z}_{jim}^q)_x^2+\frac{1}{\sigma_y^2}(\mathbf{z}_{jim}^q)_y^2+\frac{1}{\sigma_z^2}(\mathbf{z}_{jim}^q)_z^2\Big) \tag{23}$$

C. The Simplified Σ_j^q in M-Cov Step

Given the simplified version of $\mathbf{C}_{P,jim}$, in the maximization step, the terms that are related with Σ_j is as follows,

$$\begin{aligned} f(\Sigma_j)&=\sum_{i,m=1}^{N_j,M}\mathbf{C}_{P,jim}+\frac{1}{2}N_{\mathbf{P}j}\log|\Sigma_j| \\ &=\sum_{i,m=1}^{N_j,M}\mathbf{C}_{P,jim}+\frac{1}{2}N_{\mathbf{P}j}\log\sigma_x^2\sigma_y^2\sigma_z^2 \\ &=\sum_{i,m=1}^{N_j,M}\mathbf{C}_{P,jim}+N_{\mathbf{P}j}\log\sigma_x\sigma_y\sigma_z \end{aligned} \tag{24}$$

The derivative of $f(\Sigma_j)$ with respect to σ_x is

$$\begin{aligned} \frac{f(\Sigma_j)}{\sigma_x}&=-\sum_{i,m=1}^{N_j,M}\alpha_{jim}^q\sigma_x^{-3}(\mathbf{z}_{jim}^q)_x^2+\frac{N_{\mathbf{P}j}}{\sigma_x} \\ &=-\sigma_x^{-3}\sum_{i,m=1}^{N_j,M}\alpha_{jim}^q(\mathbf{z}_{jim}^q)_x^2+\frac{N_{\mathbf{P}j}}{\sigma_x} \end{aligned} \tag{25}$$

Let $\frac{f(\Sigma_j)}{\sigma_x} = 0$, we can get the expression of the updated σ_x^q as

$$\sigma_x^q = \Big(\frac{1}{N_{\mathbf{P}j}} \sum_{i,m=1}^{N_j,M} \alpha_{jim}^q (\mathbf{z}_{jim}^q)_x^2\Big)^{\frac{1}{2}} \tag{26}$$

Similarly, we can easily get the updated σ_y^2 and σ_z^2 as

$$\begin{cases} \sigma_y^q = \Big(\frac{1}{N_{\mathbf{P}j}} \sum_{i,m=1}^{N_j,M} \alpha_{jim}^q (\mathbf{z}_{jim}^q)_y^2\Big)^{\frac{1}{2}} \\ \sigma_z^q = \Big(\frac{1}{N_{\mathbf{P}j}} \sum_{i,m=1}^{N_j,M} \alpha_{jim}^q (\mathbf{z}_{jim}^q)_z^2\Big)^{\frac{1}{2}} \end{cases} \tag{27}$$

D. The Simplified $\mathbf{y}_m^q$ in M-Model Step

The simplified version of $\mathbf{y}_m^q$ can be acquired by substituting the expression of σ_x^q, σ_y^q and σ_z^q into the expression of $\mathbf{y}_m^q$ in (12).

APPENDIX E
THE RODRIGUES FORMULA

More explicitly, as that in [60], a random rotation matrix $\mathbf{R}(\boldsymbol{\theta})$ is expressed as:

$$\mathbf{R}(\boldsymbol{\theta}) = \mathbf{I}_{3\times 3} + \frac{\sin(\boldsymbol{\theta})}{||\boldsymbol{\theta}||} sk(\boldsymbol{\theta}) + \frac{1-\cos(\boldsymbol{\theta})}{||\boldsymbol{\theta}||^2} sk(\boldsymbol{\theta})^2, \tag{28}$$

where $||\bullet||$ denotes the norm of a vector or a matrix, and $sk(\boldsymbol{\theta}) \in \mathbb{R}^{3\times 3}$ is a skew-symmetric matrix:

$$sk(\boldsymbol{\theta}) = \begin{bmatrix} 0 & -\theta_3 & \theta_2 \\ \theta_3 & 0 & -\theta_1 \\ -\theta_2 & \theta_1 & 0 \end{bmatrix}. \tag{29}$$

APPENDIX F
DETAILED RESULTS OF EXPERIMENT I

In this section, we show all the detailed results of registering multiple point sets in both cases of isotropic and anisotropic positional noise. Fig. 10 (a) (b) (c) respectively show the registration error values associated with view 2, 3, 4 in the case of isotropic positional noise. Fig. 10 (d) (e) (f) respectively show the registration error values associated with view 2, 3, 4 in the case of anisotropic positional noise. In the case of isotropic positional noise, as shown in Fig. 10 (a) (b) (c), both HMM(Iso) and our proposed method outperform the other two registration approaches significantly for all three views. Our proposed method achieves comparable performances against HMM(Iso) in most test cases of different outlier percentages. These results are reasonable and indicate that our method actually reduces to HMM(Iso) in the case of isotropic positional noise. In the case of anisotropic positional noise, as shown in Fig. 10 (d) (e) (f), both HMM(Iso) and our proposed method outperform the other two approaches significantly for all three views. In terms of registration error values associated with view2, our proposed method outperforms HMM(Iso) significantly. In terms of registration error values associated with view3 and view4, our method is slightly better than HMM(Iso) in most test cases of different outlier percentages.

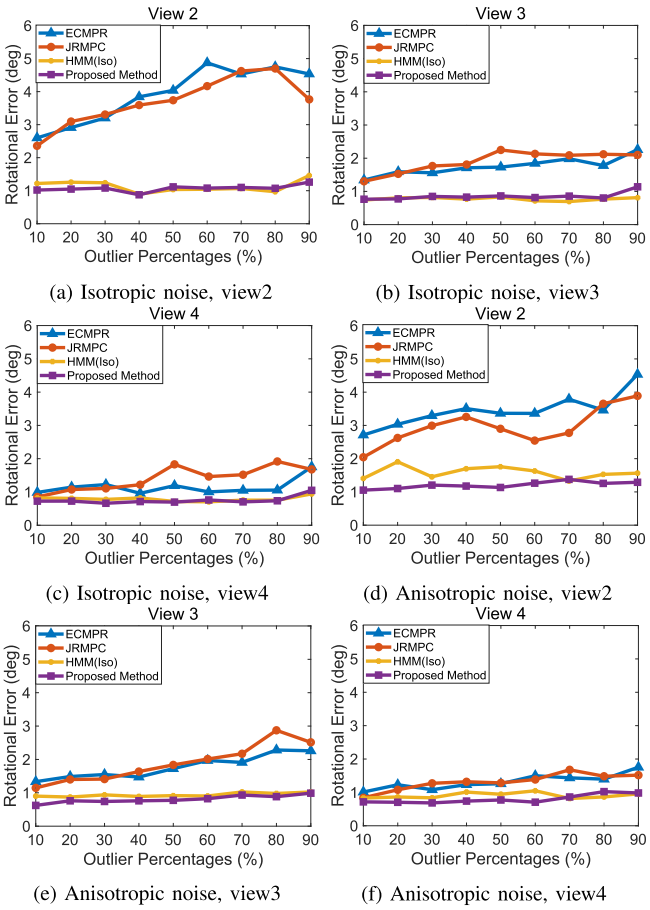

(a) Isotropic noise, view2 (b) Isotropic noise, view3
(c) Isotropic noise, view4 (d) Anisotropic noise, view2
(e) Anisotropic noise, view3 (f) Anisotropic noise, view4

Fig. 10. The mean registration error values associated with three views in the case of registering multiple point sets where isotropic positional noise and anisotropic positional noise are injected respectively. The results in all sub-figures are of the cases (a) isotropic positional noise, view 2; (b) isotropic positional noise, view 3; (c) isotropic positional noise, view 4; (d) anisotropic positional noise, view 2; (e) anisotropic positional noise, view 3; (f) anisotropic positional noise, view 4.

These results demonstrate the evident advantage of considering the anisotropic positional noise in registering multiple point sets simultaneously.

ACKNOWLEDGMENT

The authors would like to thank deeply the anonymous reviewers for their precious and constructive comments, which help a lot improve the quality of this article.

REFERENCES

[1] J. Ma, Y. Ma, and C. Li, "Infrared and visible image fusion methods and applications: A survey," *Inf. Fusion*, vol. 45, pp. 153–178, Jan. 2019.
[2] Z. Min, J. Wang, and M. Q.-H. Meng, "Robust generalized point cloud registration using hybrid mixture model," in *Proc. IEEE Int. Conf. Robot. Autom. (ICRA)*, May 2018, pp. 4812–4818.
[3] B. Maiseli, Y. Gu, and H. Gao, "Recent developments and trends in point set registration methods," *J. Vis. Commun. Image Represent.*, vol. 46, pp. 95–106, Jul. 2017.
[4] H. Li, X. He, D. Tao, Y. Tang, and R. Wang, "Joint medical image fusion, denoising and enhancement via discriminative low-rank sparse dictionaries learning," *Pattern Recognit.*, vol. 79, pp. 130–146, Jul. 2018.
[5] D. Tao, X. Lin, L. Jin, and X. Li, "Principal component 2-D long short-term memory for font recognition on single Chinese characters," *IEEE Trans. Cybern.*, vol. 46, no. 3, pp. 756–765, Mar. 2016.

[6] Y. Guo, D. Tao, W. Liu, and J. Cheng, "Multiview Cauchy estimator feature embedding for depth and inertial sensor-based human action recognition," *IEEE Trans. Syst., Man, Cybern. Syst.*, vol. 47, no. 4, pp. 617–627, Apr. 2017.

[7] C. Deng, X. Liu, C. Li, and D. Tao, "Active multi-kernel domain adaptation for hyperspectral image classification," *Pattern Recognit.*, vol. 77, pp. 306–315, May 2018.

[8] J. Ma, X. Jiang, J. Jiang, and Y. Gao, "Feature-guided Gaussian mixture model for image matching," *Pattern Recognit.*, vol. 92, pp. 231–245, Aug. 2019.

[9] J. Ma, J. Wu, J. Zhao, J. Jiang, H. Zhou, and Q. Z. Sheng, "Nonrigid point set registration with robust transformation learning under manifold regularization," *IEEE Trans. Neural Netw. Learn. Syst.*, vol. 30, no. 12, pp. 3584–3597, Dec. 2019.

[10] J. Ma, J. Zhao, J. Jiang, H. Zhou, and X. Guo, "Locality preserving matching," *Int. J. Comput. Vis.*, vol. 127, no. 5, pp. 512–531, 2019.

[11] J. Ma, X. Jiang, J. Jiang, J. Zhao, and X. Guo, "LMR: Learning a two-class classifier for mismatch removal," *IEEE Trans. Image Process.*, vol. 28, no. 8, pp. 4045–4059, Aug. 2019.

[12] A. P. Bustos and T.-J. Chin, "Guaranteed outlier removal for rotation search," in *Proc. IEEE Int. Conf. Comput. Vis. (ICCV)*, Dec. 2015, pp. 2165–2173.

[13] A. P. Bustos and T.-J. Chin, "Guaranteed outlier removal for point cloud registration with correspondences," *IEEE Trans. Pattern Anal. Mach. Intell.*, vol. 40, no. 12, pp. 2868–2882, Dec. 2018.

[14] P. Jauer, I. Kuhlemann, R. Bruder, A. Schweikard, and F. Ernst, "Efficient registration of high-resolution feature enhanced point clouds," *IEEE Trans. Pattern Anal. Mach. Intell.*, vol. 41, no. 5, pp. 1102–1115, May 2019.

[15] H. Le, T.-T. Do, T. Hoang, and N.-M. Cheung, "SDRSAC: Semidefinite-based randomized approach for robust point cloud registration without correspondences," 2019, *arXiv:1904.03483*.

[16] Z. Min, H. Ren, and M. Q.-H. Meng, "TTRE: A new type of error to evaluate the accuracy of a paired-point rigid registration," in *Proc. IEEE/RSJ Int. Conf. Intell. Robots Syst. (IROS)*, Sep. 2017, pp. 953–960.

[17] E. C. S. Chen, B. Ma, and T. M. Peters, "Contact-less stylus for surgical navigation: Registration without digitization," *Int. J. Comput. Assist. Radiol. Surg.*, vol. 12, no. 7, pp. 1231–1241, Jul. 2017.

[18] J. Wang, M. Q. H. Meng, and H. Ren, "Towards occlusion-free surgical instrument tracking: A modular monocular approach and an agile calibration method," *IEEE Trans. Autom. Sci. Eng.*, vol. 12, no. 2, pp. 588–595, Apr. 2015.

[19] A. K. Srivastava, L. Qiu, X. Xiao, C. M. Lim, and H. Ren, "Preoperative-image guided neurosurgical navigation procedures with electromagnetic tracking: An effective pipeline and a cadaver study," in *Proc. 3rd Int. Conf. Adv. Robot. Mechatronics (ICARM)*, Jul. 2018, pp. 474–479.

[20] S. Song, C. Zhang, L. Liu, and M. Q.-H. Meng, "Preliminary study on magnetic tracking-based planar shape sensing and navigation for flexible surgical robots in transoral surgery: Methods and phantom experiments," *Int. J. Comput. Assist. Radiol. Surg.*, vol. 13, no. 2, pp. 241–251, Feb. 2018.

[21] J. Wang, S. Song, H. Ren, C. M. Lim, and M. Q.-H. Meng, "Surgical instrument tracking by multiple monocular modules and a sensor fusion approach," *IEEE Trans. Autom. Sci. Eng.*, vol. 16, no. 2, pp. 629–639, Apr. 2019.

[22] L. Maier-Hein *et al.*, "Convergent iterative closest-point algorithm to accomodate anisotropic and inhomogenous localization error," *IEEE Trans. Pattern Anal. Mach. Intell.*, vol. 34, no. 8, pp. 1520–1532, Aug. 2012.

[23] H. Ren *et al.*, "Computer-assisted transoral surgery with flexible robotics and navigation technologies: A review of recent progress and research challenges," *Crit. Rev. Biomed. Eng.*, vol. 41, nos. 4–5, pp. 365–391, 2013.

[24] H. Ren, D. Rank, M. Merdes, J. Stallkamp, and P. Kazanzides, "Multisensor data fusion in an integrated tracking system for endoscopic surgery," *IEEE Trans. Inf. Technol. Biomed.*, vol. 16, no. 1, pp. 106–111, Jan. 2012.

[25] A. Rasoulian, R. Rohling, and P. Abolmaesumi, "Group-wise registration of point sets for statistical shape models," *IEEE Trans. Med. Imag.*, vol. 31, no. 11, pp. 2025–2034, Nov. 2012.

[26] N. Ravikumar, "A probabilistic framework for statistical shape models and atlas construction: Application to neuroimaging," Ph.D. dissertation, Dept. Mech. Eng., Univ. Sheffield, Sheffield, U.K., 2017.

[27] K. Wu, Z. J. Daruwalla, K. L. Wong, D. Murphy, and H. Ren, "Development and selection of Asian-specific humeral implants based on statistical atlas: Toward planning minimally invasive surgery," *Int. J. Comput. Assist. Radiol. Surg.*, vol. 10, no. 8, pp. 1333–1345, Aug. 2015.

[28] K. Jordan and P. Mordohai, "A quantitative evaluation of surface normal estimation in point clouds," in *Proc. IEEE/RSJ Int. Conf. Intell. Robots Syst.*, Sep. 2014, pp. 4220–4226.

[29] S. Billings and R. Taylor, "Generalized iterative most likely oriented-point (G-IMLOP) registration," *Int. J. Comput. Assist. Radiol. Surg.*, vol. 10, no. 8, pp. 1213–1226, 2015.

[30] Z. Min, D. Zhu, and M. Q.-H. Meng, "Accuracy assessment of an N-ocular motion capture system for surgical tool tip tracking using pivot calibration," in *Proc. IEEE Int. Conf. Inf. Autom. (ICIA)*, Aug. 2016, pp. 1630–1634.

[31] Z. Min and M. Q.-H. Meng, "General first-order TRE model when using a coordinate reference frame for rigid point-based registration," in *Proc. IEEE 14th Int. Symp. Biomed. Imag. (ISBI)*, Apr. 2017, pp. 169–173.

[32] F. Bernard *et al.*, "Shape-aware surface reconstruction from sparse 3D point-clouds," *Med. Image Anal.*, vol. 38, pp. 77–89, May 2017.

[33] A. Myronenko and X. Song, "Point set registration: Coherent point drift," *IEEE Trans. Pattern Anal. Mach. Intell.*, vol. 32, no. 12, pp. 2262–2275, Dec. 2010.

[34] G. D. Evangelidis and R. Horaud, "Joint alignment of multiple point sets with batch and incremental expectation-maximization," *IEEE Trans. Pattern Anal. Mach. Intell.*, vol. 40, no. 6, pp. 1397–1410, Jun. 2018.

[35] B. Jian and B. C. Vemuri, "Robust point set registration using Gaussian mixture models," *IEEE Trans. Pattern Anal. Mach. Intell.*, vol. 33, no. 8, pp. 1633–1645, Aug. 2011.

[36] R. Horaud, F. Forbes, M. Yguel, G. Dewaele, and J. Zhang, "Rigid and articulated point registration with expectation conditional maximization," *IEEE Trans. Pattern Anal. Mach. Intell.*, vol. 33, no. 3, pp. 587–602, Mar. 2011.

[37] G. Blais and M. D. Levine, "Registering multiview range data to create 3D computer objects," *IEEE Trans. Pattern Anal. Mach. Intell.*, vol. 17, no. 8, pp. 820–824, Aug. 1995.

[38] T. Masuda and N. Yokoya, "A robust method for registration and segmentation of multiple range images," *Comput. Vis. Image Understand.*, vol. 61, no. 3, pp. 295–307, 1995.

[39] Y. Chen and G. Medioni, "Object modelling by registration of multiple range images," *Image Vis. Comput.*, vol. 10, no. 3, pp. 145–155, Apr. 1992.

[40] V. M. Govindu and A. Pooja, "On averaging multiview relations for 3D scan registration," *IEEE Trans. Image Process.*, vol. 23, no. 3, pp. 1289–1302, Mar. 2014.

[41] R. Hartley, J. Trumpf, Y. Dai, and H. Li, "Rotation averaging," *Int. J. Comput. Vis.*, vol. 103, no. 3, pp. 267–305, Jul. 2013.

[42] V. M. Govindu, "Combining two-view constraints for motion estimation," in *Proc. IEEE Comput. Soc. Conf. Comput. Vis. Pattern Recognit. (CVPR)*, Dec. 2001, p. 2.

[43] B. Eckart, K. Kim, and J. Kautz, "HGMR: Hierarchical Gaussian mixtures for adaptive 3D registration," in *Proc. Eur. Conf. Comput. Vis. (ECCV)*, 2018, pp. 705–721.

[44] B. Eckart, K. Kim, and K. Jan, "EOE: Expected overlap estimation over unstructured point cloud data," in *Proc. Int. Conf. 3D Vis. (3DV)*, Sep. 2018, pp. 747–755.

[45] W. Gao and R. Tedrake, "FilterReg: Robust and efficient probabilistic point-set registration using Gaussian filter and twist parameterization," 2018, *arXiv:1811.10136*.

[46] J. Williams and M. Bennamoun, "Simultaneous registration of multiple corresponding point sets," *Comput. Vis. Image Understand.*, vol. 81, no. 1, pp. 117–142, 2001.

[47] N. Ravikumar, A. Gooya, A. F. Frangi, and Z. A. Taylor, "Generalised coherent point drift for group-wise registration of multi-dimensional point sets," in *Proc. Int. Conf. Med. Image Comput. Comput.-Assist. Intervent*. Cham, Switzerland: Springer, 2017, pp. 309–316.

[48] S. Bayer *et al.*, "Registration of vascular structures using a hybrid mixture model," *Int. J. Comput. Assist. Radiol. Surg.*, vol. 14, no. 9, pp. 1507–1516, 2019.

[49] A. Sinha, M. Ishii, G. D. Hager, and R. H. Taylor, "Endoscopic navigation in the clinic: Registration in the absence of preoperative imaging," *Int. J. Comput. Assist. Radiol. Surg.*, vol. 14, no. 9, pp. 1495–1506, 2019.

[50] M. Khoury, Q.-Y. Zhou, and V. Koltun, "Learning compact geometric features," in *Proc. IEEE Int. Conf. Comput. Vis. (ICCV)*, Oct. 2017, pp. 153–161.

[51] H. Deng, T. Birdal, and S. Ilic, "PPF-FoldNet: Unsupervised learning of rotation invariant 3D local descriptors," in *Proc. Eur. Conf. Comput. Vis. (ECCV)*, Sep. 2018, pp. 602–618.
[52] Z. J. Yew and G. H. Lee, "3DFeat-Net: Weakly supervised local 3D features for point cloud registration," in *Proc. Eur. Conf. Comput. Vis.*, Springer, 2018, pp. 630–646.
[53] G. D. Pais, S. Ramalingam, V. M. Govindu, J. C. Nascimento, R. Chellappa, and P. Miraldo, "3DRegNet: A deep neural network for 3D point registration," 2019, *arXiv:1904.01701*.
[54] H. Deng, T. Birdal, and S. Ilic, "PPFNet: Global context aware local features for robust 3D point matching," in *Proc. IEEE/CVF Conf. Comput. Vis. Pattern Recognit.*, Jun. 2018, pp. 195–205.
[55] Z. Gojcic, C. Zhou, J. D. Wegner, and A. Wieser, "The perfect match: 3D point cloud matching with smoothed densities," 2018, *arXiv:1811.06879*.
[56] H. Yang, J. Shi, and L. Carlone, "Teaser: Fast and certifiable point cloud registration," *IEEE Trans. Robot.*, vol. 37, no. 2, pp. 314–333, Apr. 2021.
[57] Z. Min, J. Wang, and M. Q.-H. Meng, "Joint rigid registration of multiple generalized point sets with hybrid mixture models," *IEEE Trans. Autom. Sci. Eng.*, vol. 17, no. 1, pp. 334–347, Jan. 2020.
[58] A. Banerjee, I. S. Dhillon, J. Ghosh, and S. Sra, "Clustering on the unit hypersphere using von Mises–Fisher distributions," *J. Mach. Learn. Res.*, vol. 6, pp. 1345–1382, Sep. 2005.
[59] C. M. Bishop, *Pattern Recognition and Machine Learning*. New York, NY, USA: Springer, 2006.
[60] Z. Min, J. Wang, S. Song, and M. Q.-H. Meng, "Robust generalized point cloud registration with expectation maximization considering anisotropic positional uncertainties," in *Proc. IEEE/RSJ Int. Conf. Intell. Robots Syst. (IROS)*, Oct. 2018, pp. 1290–1297.

Zhe Min (Member, IEEE) received the Ph.D. degree in electronic engineering from The Chinese University of Hong Kong, Hong Kong, in 2019.

He was a Post-Doctoral Fellow with the Department of Electronic Engineering, The Chinese University of Hong Kong (CUHK), Hong Kong. He is currently a Research Fellow of Artificial Intelligence for Surgical and Interventional Sciences with the University College London (UCL), London, U.K. His research interests include surgical navigation, medical robotics, and surface registration algorithm. He is currently serving as an Associate Editor for IEEE ROBOTICS AND AUTOMATION LETTERS (RAL).

Jiaole Wang (Member, IEEE) received the B.E. degree in mechanical engineering from the Beijing Information Science and Technology University, Beijing, China, in 2007, the M.E. degree from the Department of Human and Artificial Intelligent Systems, University of Fukui, Fukui, Japan, in 2010, and the Ph.D. degree from the Department of Electronic Engineering, The Chinese University of Hong Kong (CUHK), Hong Kong, in 2016.

He was a Research Fellow with the Pediatric Cardiac Bioengineering Laboratory, Department of Cardiovascular Surgery, Boston Children's Hospital and Harvard Medical School, Boston, MA, USA. He is currently an Associate Professor with the School of Mechanical Engineering and Automation, Harbin Institute of Technology, Shenzhen, China.

Max Q.-H. Meng (Fellow, IEEE) received the Ph.D. degree in electrical and computer engineering from the University of Victoria, Victoria, BC, Canada, in 1992.

He has been a Professor of Electronic Engineering with The Chinese University of Hong Kong (CUHK), Hong Kong, since 2002, after being the Director of the Advanced Robotics and Teleoperation (ART) Laboratory and a Professor for ten years with the Department of Electrical and Computer Engineering, University of Alberta, Edmonton, AB, Canada. He is currently the Chair of the Department of Electronic Engineering, CUHK. He is also a Distinguished Professor with the State Key Laboratory of Robotics and Systems, Harbin Institute of Technology, Harbin, China, a Distinguished Provincial Professor with the Henan University of Science and Technology, Luoyang, China, and the Honorary Dean with the School of Control Science and Engineering, Shandong University, Jinan, China. He has authored over 500 journals and conference papers. His current research interests include robotics, perception and sensing, human–robot interaction, active medical devices, biosensors and sensor networks, and adaptive and intelligent systems.

Dr. Meng is an Elected Member of the Administrative Committee of the IEEE Robotics and Automation Society. He has served on many editorial boards. He was a recipient of the IEEE Millennium Medal and a Fellow of the Hong Kong Institution of Engineers and the Canadian Academy of Engineering.